GEOPHYSICS, VOL. 43, NO. 1 (FEBRUARY 1978); P. 49–76, 37 FIGS.

INTEGRAL FORMULATION FOR MIGRATION IN TWO AND THREE DIMENSIONS

WILLIAM A. SCHNEIDER*

Computer migration of seismic data emerged in the late 1960s as a natural outgrowth of manual migration techniques based on wavefront charts and diffraction curves. Summation (integration) along a diffraction hyperbola was recognized as a way to automate the familiar point-to-point coordinate transformation performed by interpreters in mapping reflections from the x, t (traveltime) domain into the x, z (depth domain).

We will discuss the mathematical formulation of migration as a solution to the scalar wave equation in which surface seismic observations are the known boundary values. Solution of this boundary value problem follows standard techniques, and the migrated image is expressed as a surface integral over the known seismic observations when areal or 3-D coverage exists. If only 2-D seismic coverage is available, wave equation migration is still possible by assuming the subsurface and hence surface recorded data do not vary perpendicular to the seismic profile. With this assumption, the surface integral reduces to a line integral over the seismic section, suitably modified to account for the implicit broadside integral. Neither the 2-D or 3-D integral migration algorithms require any approximation to the scalar wave equation. The only limitations imposed are those of space and time sampling, and accurate knowledge of the velocity field.

Migration can also be viewed as a downward continuation operation which transforms surface recorded data to a deeper hypothetical recording surface. This transformation is convolutional in nature and the transfer functions in both two and three dimensions are developed and discussed in terms of their characteristic properties. Simple analytic and computer model data are migrated to illustrate the basic properties of migration and the fidelity of the integral method. Finally, applications of these algorithms to field data in both two and three dimensions are presented and discussed in terms of their impact on the seismic image.

INTRODUCTION

Migration of seismic data has been a basic tool of interpreters since at least the 1940s. The classic work of Hagedoorn (1954) provided firm theoretical basis for the migration of time sections in two or three dimensions based upon the use of wavefront charts and diffraction curves. In the late 1960s, numerous computer implementations of Hagedoorn's migration principle became available for commercial use in seismic data processing. In the main, these programs accomplished migration by summation of stacked trace amplitudes along hyperbolic trajectories governed by the rms velocity distribution.

A recent revival in migration theory and practice stems principally from the work of Jon Claerbout (1970, 1972) and his colleagues at Stanford University, who first formulated a finite-difference algorithm for migration based upon the scalar wave equation. Commercial programs are now available in industry to implement finite-difference migration of seismic data based on Claerbout's original work and extensions thereof. These techniques are variously called "wave equation" migrations.

This paper develops an alternate view of wave equation migration in which the problem is posed as a boundary value problem, which leads naturally to

Presented at the 46th Annual International SEG Meeting, October 24, 1976 in Houston. Manuscript received by the Editor January 7, 1977; revised manuscript received June 26, 1977.
*Formerly Texas Instruments, Dallas, TX.; currently Colorado School of Mines, Golden, CO 80401.

an integral or summation algorithm for migration in either two or three dimensions. As will be seen, the integral solution has strong historic ties to the "conventional" diffraction summation approach of the late 1960s. The differences are subtle but significant in terms of amplitude and waveform reconstruction, faithful to the scalar wave equation.

THEORY

For completeness, the integral migration algorithm will be derived from first principles starting with the scalar wave equation,

$$\nabla^2 U - \frac{1}{C^2} U_{tt} = -4\pi q(r, t).$$

The complete solution to the inhomogeneous wave equation in an arbitrary volume V_0 is given by a surface integral on S_0 enclosing V_0 involving the boundary values, and a volume integral over V_0 involving both source terms and initial values. This result is well known in the mathematical physics literature (see, for example, Morse and Feshback, 1953) and derives from an application of Green's theorem. For our purposes, the volume integral may be ignored since the initial values are assumed to be zero before the shot instant, and there are no real sources in the subsurface image space, just reflectors and scatterers. Thus, we are left with the homogeneous wave equation and inhomogeneous boundary conditions of the Dirichlet type. The remaining surface integral is given by,

$$U(r, t) = \frac{1}{4\pi} \int dt_0 \int dS_0 \left[G \frac{\partial}{\partial n} U(r_0, t_0) - U(r_0, t_0) \frac{\partial}{\partial n} G \right]. \quad (2)$$

The specific geometry of interest is shown in Figure 1 with $\mathbf{n}$ the outward normal vector to the surface S_0. It includes the recording surface $Z = 0$ place, and a hemisphere extending to infinity in the subsurface. Contributions from the distant hemisphere are ignored, and the boundary value representation reduces to an integral over the surface involving the wave field on S_0 and a suitable Green's function G. Since $U(r_0, t_0)$ in equation (2) is equated to the observed seismic data, we require that $G = 0$ on S_0 in order to eliminate the gradient of U, which may not also be independently specified, nor is it measured in current seismic practice. A Green's function having the desired properties at the free surface consists of a point source at r_0 and its negative image at r_0', or

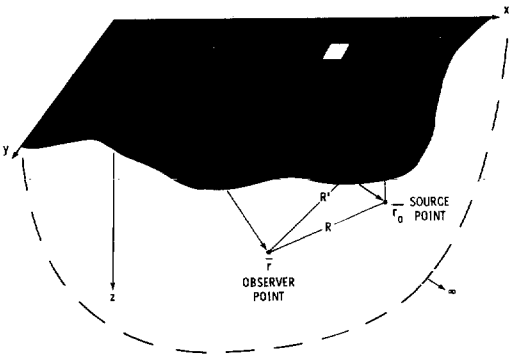

FIG. 1. Geometry for boundary value solution.

$$G(r, t|r_0, t_0) = \frac{\delta\left(t - t_0 - \frac{R}{C}\right)}{R} - \frac{\delta\left(t - t_0 - \frac{R'}{C}\right)}{R'}, \quad (3)$$

where

$$R = \sqrt{(z - z_0)^2 + (x - x_0)^2 + (y - y_0)^2},$$

and

$$R' = \sqrt{(z + z_0)^2 + (x - x_0)^2 + (y - y_0)^2}.$$

Other choices of G are possible for image reconstruction purposes as discussed by Kuhn and Alhilali (1976). Substitution of equation (3) into equation (2) and simplification yields the following integral representation for the wave field $U(r, t)$ at any point in image space in terms of observations of the wave field $U(r_0, t_0)$ on the surface,

$$\cdot U(r, t) = \frac{1}{2\pi} \int dt_0 \int dA_0 \cdot U(r_0, t_0) \frac{\partial}{\partial z_0} \left[\frac{\delta\left(t - t_0 - \frac{R}{C}\right)}{R} \right]. \quad (4)$$

This is a rigorous statement of Huygen's principle and is commonly called the Kirchhoff integral. From the form of the kernel of equation (4), we recognize the transformation as a three-dimensional convolution of the observed wave field with a space-time operator related to the point source solution to the wave equation. We will return to this point subsequently. Before doing so, however, it is instructive to re-express equation (4) by performing the indicated Z_0 differentiation and t_0 integration resulting in an equivalent expression.

$$U(r,t)=\frac{1}{2\pi}\int dA_0\frac{\cos\theta}{RC}\left[U'(r_0,t_0)+\frac{C}{R}U(r_0,t_0)\right]_{t_0=t-(R/C)}. \tag{5}$$

The bracketed term contains the time derivative of the recorded data plus the recorded data scaled by C/R or $1/t$ the reciprocal traveltime, all evaluated at the "retarded" time $t_0=t-R/C$. Multiplying the brackets is the familiar "obliquity" factor, $\cos\theta$. Because of the $1/t$ multiplier, the second term in brackets is frequently dropped giving the Rayleigh-Sommerfeld diffraction formula of optics, Goodman (1968). However, it is no problem to retain both terms in seismic applications; we need only to differentiate the seismic section and add to it the same section scaled by $1/t$ in order to implement equation (5) exactly. Trorey (1970), Hilterman (1970, 1975), and Berryhill (1976) make extensive use of the Kirchhoff integral [equation (5)] in forward modeling studies of diffraction and other propagation complexities in two and three dimensions. For a lucid discussion of the historic role of equation (5) and its many variants in optical, acoustic, and seismic imagery, the author recommends the excellent treatment given by Walter and Peterson (1976).

Still another representation of equation (4) is possible by interchanging the Z_0 derivative with a Z derivative which may then be taken outside the integral, giving

$$U(r,t)=-\frac{1}{\pi}\frac{\partial}{\partial z}\int dA_0\frac{U\left(r_0,t-\frac{R}{C}\right)}{R}. \tag{6}$$

This is the most compact form and clearly demonstrates that the integral transformation is a solution to the 3-D wave equation by virtue of the form of the kernel $f(t-R/C)/R$. Now let us return to the convolutional aspects of this transformation. As noted previously, the integral transformation equation (4) may be written symbolically as a three-dimensional convolution,

$$U(x,y,z,t)=U(x,y,z_0,t)*\frac{1}{2\pi}\frac{\partial}{\partial z_0}\left[\frac{\delta\left(t\pm\frac{r}{C}\right)}{r}\right], \tag{7}$$

where

$$r^2=\Delta z^2+x^2+y^2,$$

which translates the observed wave field from one

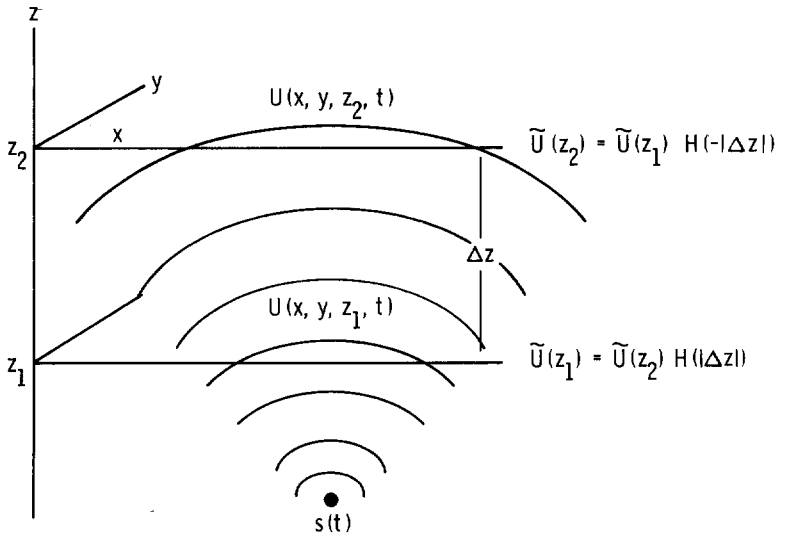

MIGRATION USES H(+|Δz|) TO EXTRAPOLATE CONVERGING WAVES

FIG. 2. Extrapolation of converging and diverging waves.

Z-plane to another. If we Fourier transform expression (7) over x, y, and t (Appendix A), the operation becomes complex multiplication in the frequency wavenumber domain, giving

$$\tilde{U}(k_x, k_y, z, \omega) = \tilde{U}(k_x, k_y, z_0, \omega)\, H(k_x, k_y, \Delta z, \omega), \quad (8)$$

where

$$H = e^{\pm i|\Delta z|}\sqrt{\left(\frac{\omega}{C}\right)^2 - k_x^2 - k_y^2}. \quad (9)$$

The transfer function H is seen to be a pure phase operator embodying the exact dispersion relation for the scalar wave equation. The operator H, expressed either in the space-time domain or frequency wavenumber domain, enables us to extrapolate waves in space, which we will see shortly is basic to seismic image reconstruction. The choice of sign in equation (7) and (8) is important insofar as it determines the direction of extrapolation. To clarify the choice, consider Figure 2 which depicts a spherical wave radiating from S and two observation surfaces at Z_1 and Z_2. The wave field at Z_2 can be obtained from the field at Z_1, which is closer to the source, by using expression (8) with the negative sign in operator H to reflect the phase delay in propagation across the slab of thickness ΔZ. Conversely, we can make the clock run backward and compute the field at Z_1 from the field at Z_2 by use of the positive sign in H to reflect the phase advance in moving a distance ΔZ closer to the source. In the operation of migration we must use the positive sign in operator H to extrapolate *converging waves* back toward their origins. With these basic mathematical tools to move data around, let us now review the principle of migration based on these integral transformations.

First, it is important to recognize that the wave field extrapolation equations developed thus far are not suitable for application to field records. While it is not difficult to pose the problem to accommodate shot-to-detector offset [see, for example, Timoshin (1970) and French (1975)], the mathematics are somewhat messier. For simplicity, we limit this discussion to the familiar CDP stack representation which approximates coincident source/receiver geometry as illustrated in Figure 3. Furthermore, the equations are cast in one-way traveltime so we can either divide our stacked section time scales by 2 or use a velocity in migration equal to 1/2 the true velocity. With these two assumptions, it becomes clear that the "physical" experiment we are approximating with stacked data is one in which the re-

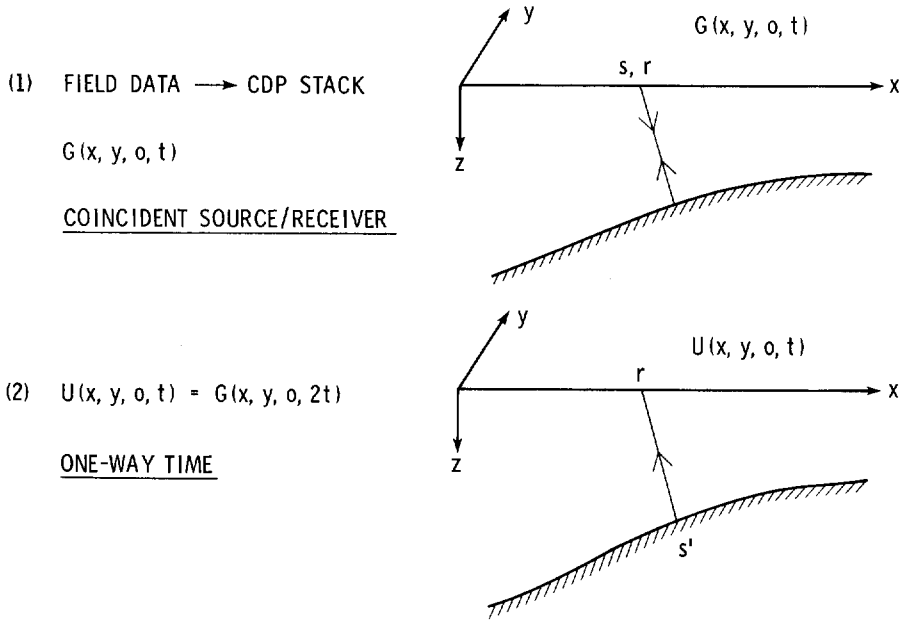

FIG. 3. Migration principle: steps 1 and 2.

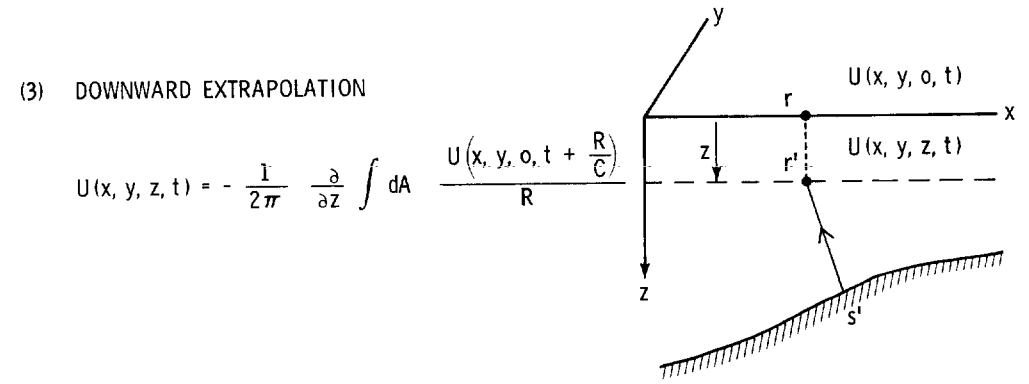

FIG. 4. Migration principle: steps 3 and 4.

ceivers are located on the surface, the sources are positioned along the reflecting interfaces, their strengths are proportional to the reflection coefficients, and they are fired in unison. That such a physical (though not necessarily practical) experiment could account for most if not all of the significant events present on a CDP stack section is of more than academic interest. Migration and other inverse wave equation processes require input data that are reasonably consistent with some forward propagation process. Not all current seismic processing techniques preserve the integrity of this forward-inverse relationship. For example, fast AGC applied either before or after stack can dramatically alter the amplitude of complex wave interferences which, if undisturbed, can be unscrambled by migration in the inverse propagation process. Thus, given that the CDP stack, properly processed, is amenable to wave equation manipulation, we next insert this data into our previously derived transformation equation to downward extrapolate the surface recorded data to successively deeper levels, as depicted in Figure 4, step 3. This in itself is not yet migration, for the equation as written would give us a time function $U(x, y, z, t)$ for each x, y, z position. Instead, we really only want to map a single value for each position, a value proportional to the reflection or scattering strength at that subsurface location, or in the context of our "physical" experiment, we wish to map the equivalent source strength at all subsurface positions at the shot instant $t = 0$. Therefore, we must fix $t = 0$ and evaluate the integral for all x, y, z of interest as indicated in step 4 of Figure 4. This is *3-D migration* for stacked data based on the Kirchhoff integral formula.

To further clarify this concept, consider Figure 5 which illustrates the input-output mapping relationship implied by the equations of Figure 4. The input assumes we have stacked data over the $Z = 0$ plane for the model shown. The output is a single trace at some x, y location plotted versus Z and vertical time Z/C. As the receiver moves down through successive positions, a point is mapped at each step by evaluating the integral with $t = 0$. For example, simulated receiver r_1 at z_1 maps a zero at $t = 0$ because the reflection has not arrived. Similarly, the response is zero at z_2, and as becomes obvious, the integral will be zero when evaluated at zero traveltime unless the receiver is sitting on top of or very near the reflector. When it is, the reflection wavelet will be mapped at the vertical traveltime below the surface receiver position (actually below the CDP midpoint position). We recognize that this mapping procedure will produce the migrated picture.

Thus far, the development has assumed seismic observations are available over an area of sufficient

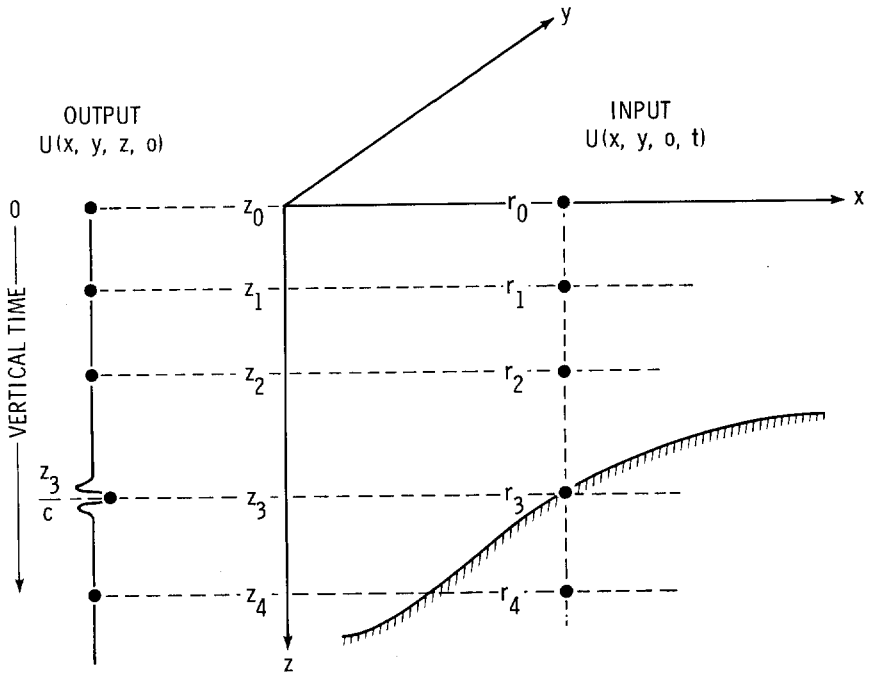

FIG. 5. Migration principle: input-output relationship.

extent to perform the indicated surface integrals or their discretized equivalents. This requires a 3-D seismic survey in which data are acquired over an entire prospect with space sampling of the order of one-half the shortest wavelengths of interest. While surveys of this kind have been and are now being conducted on a limited scale, the bulk of current seismic information is still 2-D, having been collected along widely spaced lines or traverses. In order to use the foregoing theory to migrate data from a single line and retain the benefits of a wave equation algorithm, we must make some assumption about the nature of the surface data $U(x, y, 0, t)$ where we did not measure it. The most common practice is to assume the wave field at the surface is only 2-D; that is, if the line was shot in the x-direction, then

$$U(x, y, 0, t) = U(x, 0, t),$$

independent of y. For this to be true, two conditions must be met: (1) the subsurface geology must be independent of y, and (2) the source must either be a line source in the y-direction or the source and receiver must be colocated as is approximately the case in CDP stack. If these conditions are met, the appropriate 2-D transfer functions can be obtained from equations (7) and (8), by either integrating out the y dependence in the 3-D space-time operator or setting $k_y = 0$ in the frequency-wave number operator. The corresponding 2-D transfer functions are given below:

$$h(x, \Delta z, t) = \frac{1}{\pi}\frac{\partial}{\partial z_0}\frac{H\left(t \pm \frac{r}{c}\right)}{\sqrt{t^2 - \left(\frac{r}{c}\right)^2}}, \qquad (10)$$

where

H = unit step function,

$$r = \sqrt{(z - z_0)^2 + x^2},$$

and

$$H(k_x, \Delta z, \omega) = e^{\pm i|\Delta z|\sqrt{\left(\frac{\omega}{c}\right)^2 - k_x^2}}. \qquad (11)$$

The resulting expressions (10) and (11) are, of course, Fourier transform pairs and bear the same relationship to the 2-D wave equation solution as the 3-D transfer functions equations (7) and (8) bear to the 3-D wave equation. The 2-D migration algorithm obtained by convolving equation (10) with $U(x, 0, t)$ and setting $t = 0$ as required by the mapping principle gives:

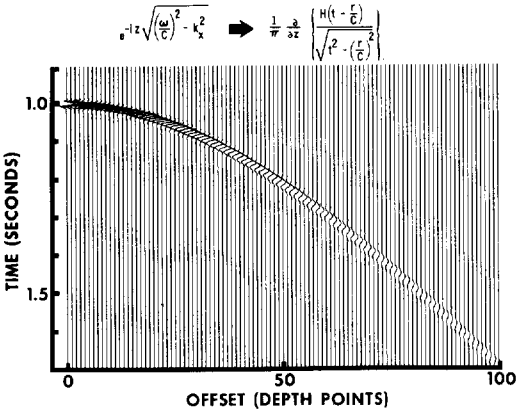

FIG. 6. Exact 2-D transfer function.

$$U(x, z, 0) = -\frac{1}{\pi}\frac{\partial}{\partial z}\int dx \int_{r/c} d\tau \frac{U(x, 0, \tau)}{\sqrt{\tau^2 - \frac{r^2}{c^2}}}. \quad (12)$$

This expression is somewhat more complicated looking than its 3-D counterpart of Figure 4, because the y integral has been replaced by a time integral along the trace. In order to more fully appreciate the relationship between the 2-D and 3-D migration expressions, consider the following hypothetical experiment. First, consider migrating a seismic section using the 2-D expression given in equation (12). Next, imagine replicating that same input section many times to simulate shooting parallel lines in the dip direction of a 2-D subsurface model. Then 3-D migrate these parallel lines using the expression in Figure 4. The results of the two migrations will be identical; that is, expression (12) actually accomplishes 3-D wave equation migration under the special circumstances that the surface recorded data are independent of one surface variable. When the above is not true, then equation (12) is not a valid migration, and as every interpreter should know, user beware!

Before leaving the mathematics of migration, it is instructive to examine the behavior of the 2-D transfer function, equation (10), in more detail. Figure 6 shows a plot one-half the exact space-time operator as it would appear when being convolved with the section for an output value at 1 sec vertical traveltime. The operator shown is band-limited in both space and time appropriate to the sampling. The hyperbolic trajectory is predictable from simple ray theory considerations; however, the amplitude and phase behavior are not. The aperture width, ± 100 traces in this example is arbitrary, and generally is chosen to accommodate the maximum geologic time dip to be migrated. In principle, dips to 90 degrees and beyond can be migrated by the integral approach; however, this is not the case for finite-difference migration algorithms. Figure 7 shows a plot of an approximate 2-D transfer function obtained from equation (11) by assuming near vertical incidence propagation which yields

$$e^{-iz\sqrt{\left(\frac{\omega}{c}\right)^2 - k_x^2}} \Rightarrow e^{-i\frac{z\omega}{c}\left(1 \;\; \frac{1}{2}\left(\frac{ck_x}{\omega}\right)^2\right)} \quad (13)$$

for

$$\frac{\omega}{c} \gg k_x.$$

This approximation is the basis of Claerbout's (1972) so-called 15 degree finite difference algorithm. The approximate operator plotted in Figure 7 and the exact operator in Figure 6 are virtually identical near the apex corresponding to small dip angles. The approximate operator decays more rapidly with offset and follows a parabolic rather than hyperbolic trajectory. Both these factors, plus frequency dispersion associated with finite differencing schemes, limit the accuracy and fidelity of finite difference migration in steeply dipping situations. While it is true that higher order approximations are possible and have been discussed by Claerbout (1976) and others, in the limit they can only approach the exact transfer function which the integral method achieves with ease. Next, let us examine the application of these migration algorithms to both model and field data.

MODEL RESULTS

First, consider the analytical migration of a plane

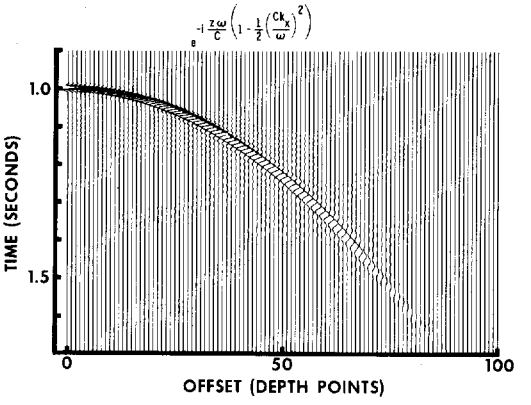

FIG. 7. Approximate 2-D transfer function.

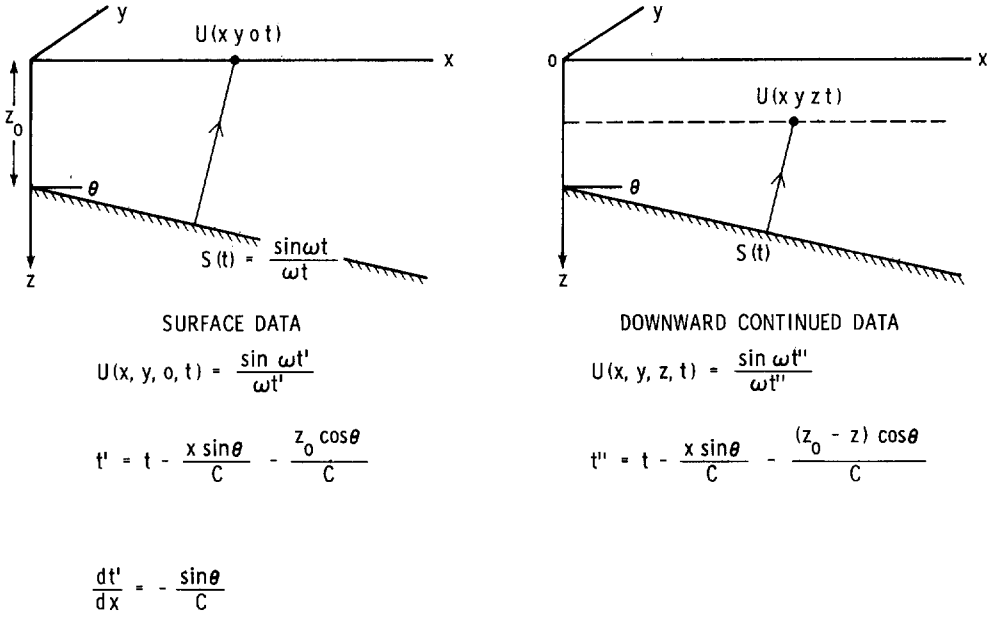

FIG. 8. Plane dipping reflector example.

dipping reflection depicted in Figure 8. On the left of the figure, we postulate a band-limited signal $S(t)$ emanating from a bed dipping at angle θ in the x, z plane. The surface recorded data $U(x, y, 0, t)$ is a delayed version of this signal, and the observed time dip dt'/dx is the familiar quantity $\sin\theta/c$. For this analytical signal we can actually analytically downward continue our receiver to a depth z using either equation (7) or (8). The result, $U(x, y, z, t)$, is not unexpected and could have been arrived at by inspection. Since the receiver is a distance z closer to the reflector, the traveltime delay is reduced by $z \cos\theta/c$. Now to obtain the migrated time picture we must invoke the mapping principle by setting $t = 0$, and change variable from depth z to vertical time $\tau = z/c$ as shown by $U(x, y, \tau, 0)$ in Figure 9. In migrated time space, the time dip $d\tau'/dx$ after migration becomes $\tan\theta/c$, and the bandwidth of the signal is reduced by $\cos\theta$. Since migration is a loss-less process, the latter is purely a geometrical effect due to rotation of the reflection. Put another way, migration increases the time dip of a reflector by $\cos\theta$ and decreases the apparent signal frequency by the same factor so as to preserve horizontal wavenumber.

Now let us examine the computer migration of several simple synthetic sections. Figure 10 models four flat reflections and four dipping reflections with time dips of 4, 8, 12, and 16 msec/trace, respectively. The reflection wavelet is a zero phase, 0–80 Hz bandwidth pulse. A 2-D migrated picture is shown in Figure 11. A trace spacing of 25 m and velocity of 2500 m/sec were used resulting in structural dips ranging from 12 to 53 degrees. The steepest event has migrated some 200 traces, or about 5 km.

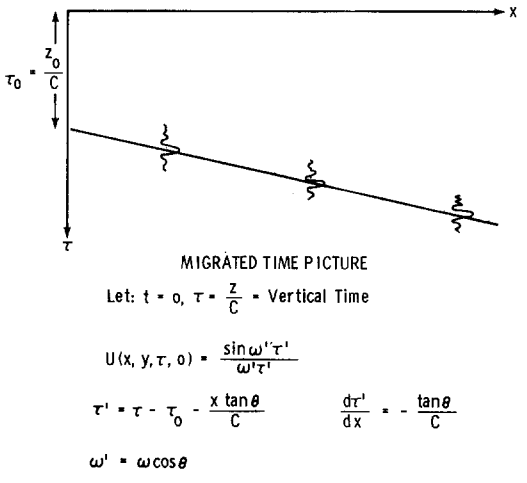

FIG. 9. Analytical migration of dipping reflector.

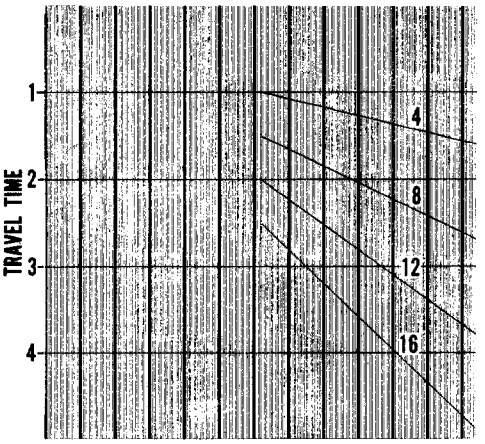

FIG. 10. Synthetic time section modeling four flat reflections and four dipping reflections at 4, 8, 12, and 16 msec/*tr* dip.

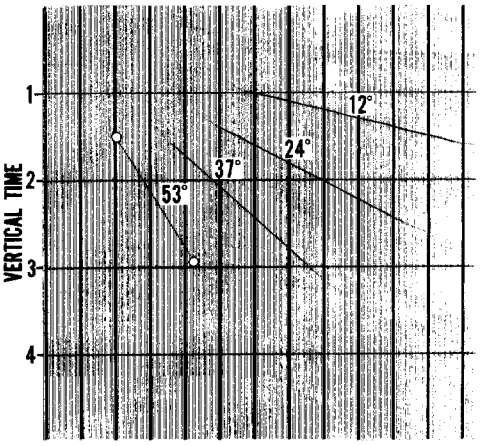

FIG. 11. 2-D migrated time section, $\Delta X = 25$ m, $V = 2500$ m/sec.

The dots on the 53 degree event indicate the predicted migrated end points for the 16 msec/trace reflection in Figure 10, the correspondence is excellent. The slight tails on each of the migrated events result from not including diffractions in the input model. The details of the result are more evident in Figures 12 and 13 which show enlarged portions of the input section and migrated section, respectively. The low level jitter on the input are sidelobes associated with the sharp cutoffs in the wavelet design. The background noise in the output is a combination of the above and migration noise. The expected results are also evident from these figures; namely, (1) the migrated dip is greater than the unmigrated dip by cos θ, and (2) the migrated pulse is reduced in apparent bandwidth by cos θ, thereby keeping the horizontal wavenumber invariant. It is also interesting to note the 12 and 16 msec/trace reflections have a significant portion of their bandwidth beyond the 1/2 wavelength Nyquist space sampling limit of 42 and 32 Hz, yet these events are properly migrated including the aliased components. The question of migrating under sampled data is more complex than one might expect, nor is it independent of the algorithm. With the integral approach it is possible to correctly migrate aliased data by not spatially bandlimiting the migration operator shown previously in Figure 6. The risk in doing this is to generate migration background noise which in the previous example is sufficiently low level to be unobjectionable. However, the effect is very sensitive to the space sampling ΔX. Figure 14 shows another migration of the input model in Figure 10 in which the trace interval was doubled to 50 m; that is, the migration program was told the ΔX was 50 m instead of 25 m, but the identical section was migrated. Of course, the implied structural picture is different, and, as before, the events are correctly migrated, including aliased frequencies. The most notable difference, however, is the increase in migration noise from both flat and

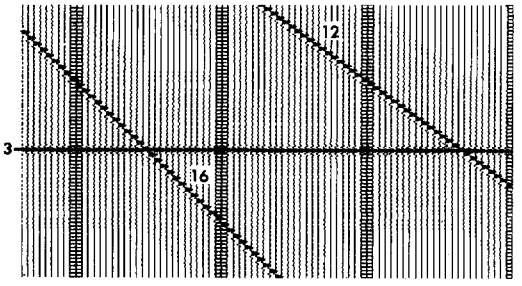

FIG. 12. Detail of input section in Figure 10.

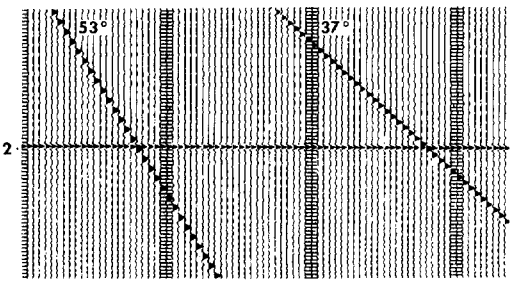

FIG. 13. Detail of migrated section in Figure 11.

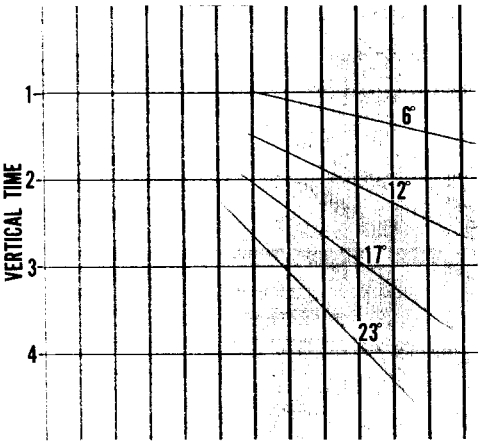

FIG. 14. 2-D migrated time section, $\Delta X = 50$ m, $V = 2500$ m/sec.

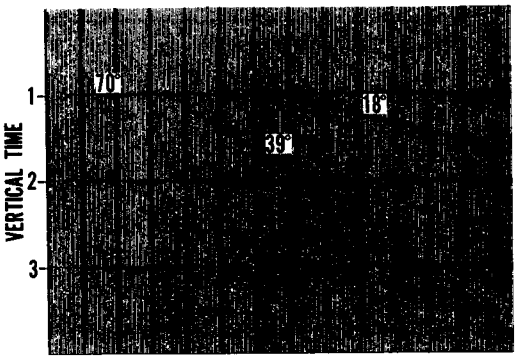

FIG. 15. 2-D migrated time section, $\Delta X = 16$ m, $V = 2500$ m/sec.

dipping events. This is basically a leakage problem caused by approximating the integral [equation (12)] by a discrete summation. The coarser the ΔX, the poorer the summation approximates the integral and the greater the leakage. While ΔX is a critical parameter, the leakage also depends on frequency, velocity, migration aperture, and traveltime. In general, the leakage worsens with increasing ΔX, increasing frequency, increasing aperture, decreasing velocity, and decreasing traveltime. The problem also scales as the ratio of $V/\Delta X$. In other words, the 50 m model with a 5000 m/sec velocity would have the same low noise level as the 25 m, 2500 m/sec migration in Figure 11. To guard against this problem on coarsely sampled data (whether or not it is aliased), the migration operator must be spatially bandlimited as in Figure 6 or, equivalently, a more sophisticated numerical integration must be used in lieu of discrete summation. Before leaving this sample plane dipping model, however, we will migrate it one more time using a ΔX of 16 m giving the result as shown in Figure 15. The third dipping event now appears as a greatly compressed 70 degree segment which has migrated some 300 traces horizontally and 1.0 to 1.5 sec in time to its correct subsurface position. The missing fourth reflection does not represent a possible reflection in this model because its 16 msec/trace time dip exceeds the maximum of 13 msec/trace for a 90 degree reflector; hence it is not imaged.

As is apparent from these examples, the integral method has no algorithmic limitations on dip. Reflections can be migrated to 90 degrees and beyond in the presence of vertical velocity gradients. The issues of velocity and cost ultimately become the limiting factors, but before addressing the questions of velocity inhomogeneity, another slightly more realistic model is of interest.

Figure 16 shows a synthetic zero offset time section for three reflecting horizons of moderate complexity computed using a forward wave theory approach described by Trorey (1970). A constant 8000 ft/sec velocity was used, the trace interval is 50 ft, and the wavelet bandwidth is approximately 0–60 Hz. Many of the classic diffraction phenomena so often seen on stacked sections are present. The 2-D integral migration shown in Figure 17 is virtually a perfect reconstruction of the subsurface acoustic impedance with accurate representation of the amplitude and waveform, structural attitude, curvature, and bed terminations. Were the world so simple, seismic processing would be a closed book. Unfortunately, real seismograms are infinitely more complex than the constant velocity model depicted here, and much progress remains to be made in seismic processing techniques before we can accurately image in heterogeneous media.

Some of the more practical aspects of migrating seismic data are knowing what velocity to use, how to estimate it from the data, and how accurate it must be. None of these are trivial issues, nor shall I attempt to provide comprehensive answers. Certainly the issues of estimating seismic velocity for stacking and more recently for migration have received ample attention in the literature and in professional society meetings. I will not attempt to summarize the current art in this mature activity except to point out there is a trend away from CDP stack based velocity analysis toward migration based techniques [Sattlegger (1975), Dohr (1975)]. The trend will undoubtedly accelerate as migration of unstacked

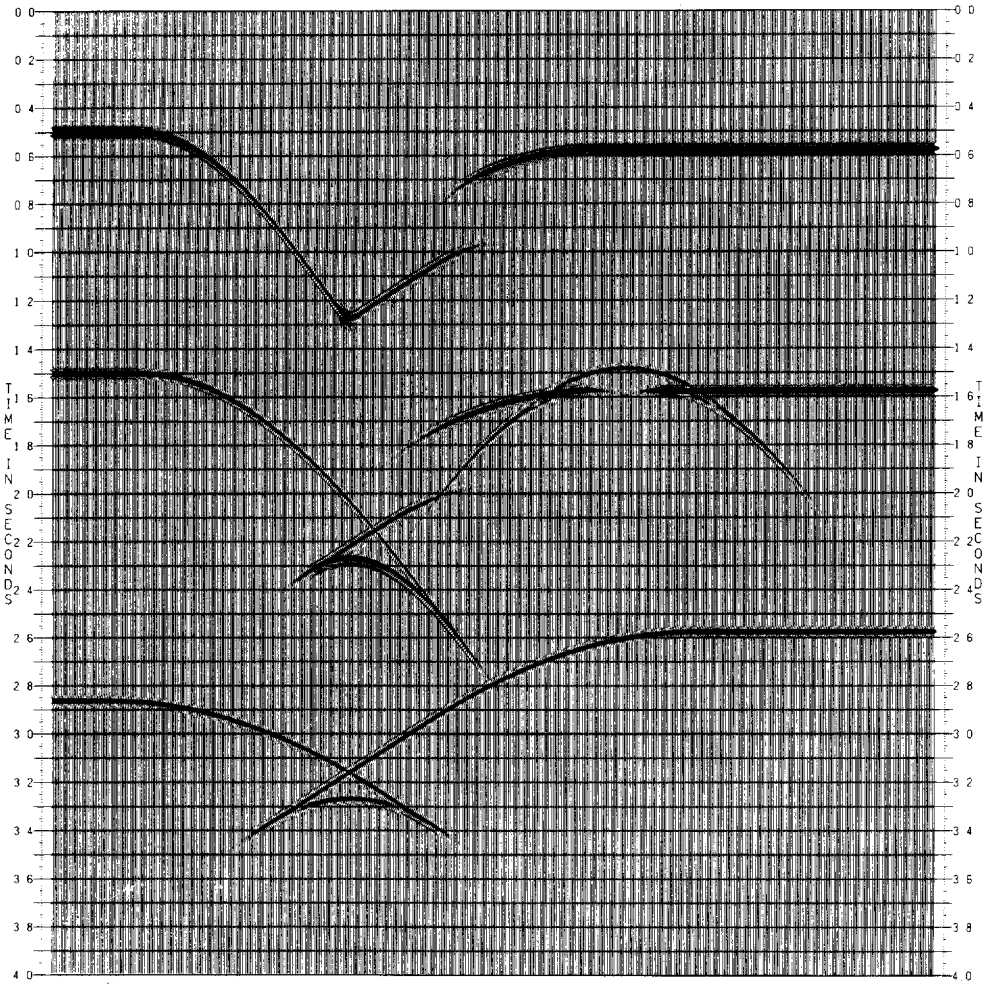

FIG. 16. Wave theory, zero offset time section modeled at 8000 ft/sec and 50 ft trace spacing.

data gradually replaces the CDP stack as the standard seismic image.

The question of (post stack) migration velocity sensitivity is somewhat more easily addressed, and I use the model in Figure 16 to illustrate the effects of slightly under and over migration. The section was remigrated with a velocity of 7600 ft/sec (5 percent low) and 8400 ft/sec (5 percent high). The results are shown in Figures 18 and 19, respectively. In a gross sense the pictures are very similar to Figure 17 migrated with the correct velocity. In detail they differ; for example, the fault terminations are blurred, the flanks of the synclines are in error by several hundred feet, and the small bump on the second reflector is severely distorted. Other distortions in amplitude and waveform are not readily discernible, and, as expected, the flat reflections are totally insensitive to velocity. While not a comprehensive answer to the velocity sensitivity question, we may readily conclude that: the more complex the subsurface, the more diffraction-like is the time section, and the more accurate must the velocity be. Even with faulted simple geology, relatively small errors in migration velocity will improperly collapse the diffraction tails and blunt fault resolution.

VELOCITY INHOMOGENEITY

In the foregoing development, starting with the scalar wave equation and resulting in integral migration algorithms based thereon, it has been tacitly assumed the techniques could be successfully applied to waves propagating in a variable velocity medium

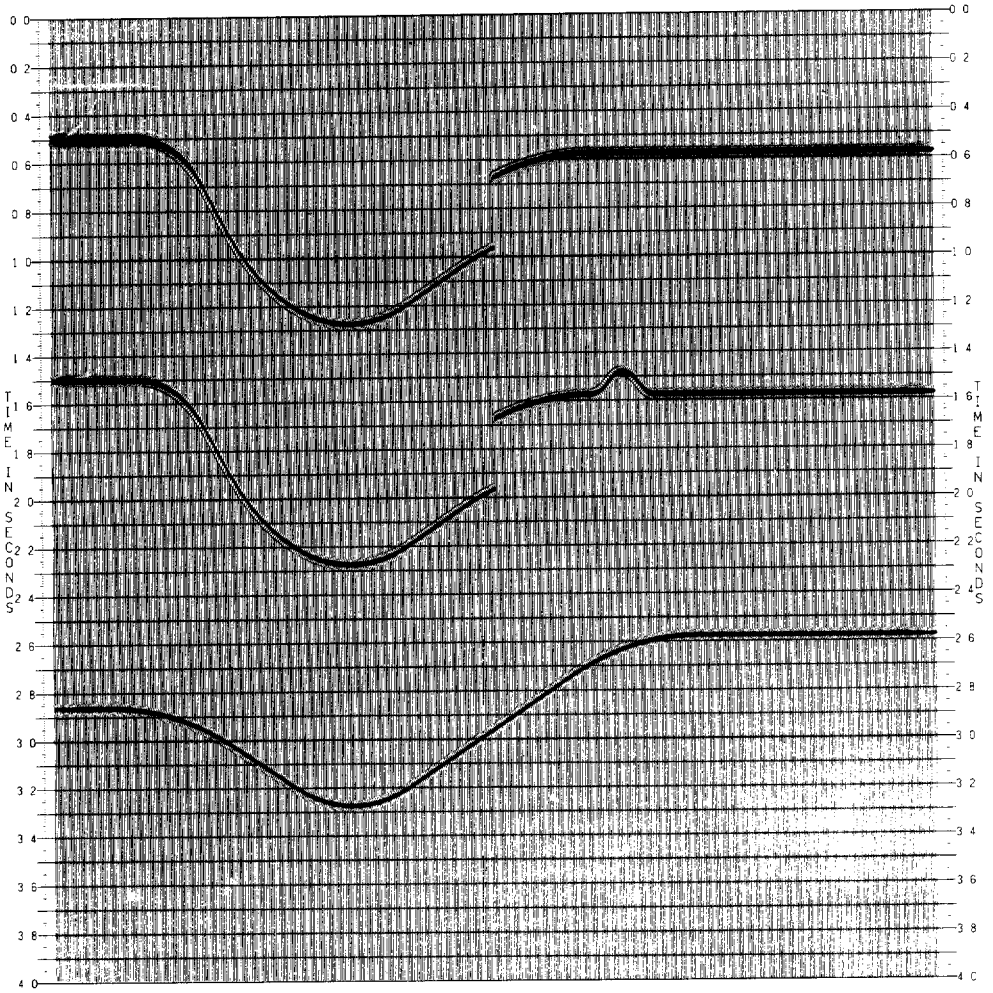

FIG. 17. 2-D migrated synthetic wave theory section.

even though the derivation assumed constant velocity. This is certainly not intuitively obvious, but as will be shown, the method is remarkedly robust with regard to vertical velocity variations.

First, consider the 2-D migration of a single sinusoidal trace with constant velocity. The result in Figure 20 shows the familiar windshield wiper pattern. The dark bands trace out the wavefronts at 2, 3, and 4 sec of traveltime. The trace amplitude decays with time to compensate for decreasing wavefront curvature, and the decay with offset along the wavefront reflects the obliquity factor $\cos\theta$. Now if we vary the velocity $C = C(z)$ for each depth or vertical time step in the migration algorithm [equation (12)], the wavefront pattern takes on a very different shape as shown in Figure 21. For this linear increasing velocity $V = 1800 + 600t$ m/sec, the wavefronts are flatter for small dip angles and swoop up more rapidly for steep dips. When the wavefront approaches vertical, the structural dip is 90 degrees. This occurs at the surface for constant velocity, but well below the surface with an increasing velocity function. The question of accuracy of the variable velocity result can best be answered from simple model studies.

The first model is described by the instantaneous, average and rms velocities shown in Figure 22. Figure 23 compares the true curved ray wavefront with those generated by the integral migration algorithm using both the average and rms velocity distributions of Figure 22. The exact curve was computed by integrating the traveltime equations as

described by Musgrave (1961). For traveltimes of 1, 2, 3, and 4 sec, the wavefronts are virtually identical for dips less than 20 degrees. The rms velocity curve continues to track the exact wavefront to about 40 degrees and then departs gradually as the dip angle increases. Even out to approximately 60 degrees the offset error is only about 1–2 percent, which implies the velocity is too slow by the same amount.

A second model, Figure 24, presents a more complicated velocity distribution consisting of a deep water layer over a high-velocity subsurface. The wavefronts shown in Figure 25 tell a similar story; the errors are slightly greater due to the large discontinuity at the water bottom, yet migration using the rms velocity appears quite satisfactory to about 60 degrees, considering the expected accuracy of seismic velocity estimation.

A final model, Figures 26 and 27, shows a first order velocity discontinuity at depth between two linearly increasing functions. The errors are of the same magnitude as in the previous two models and suggests that for this class of linear increasing velocity functions (with or without discontinuities), the strategy of using the vertical rms velocity in the integral migration algorithm [equation (12)] will produce quite accurate migrations to the order of 60 degrees structural dip. The errrors increase with angle and total distance traveled. At early times, less than 2 sec for these models, accurate migrations

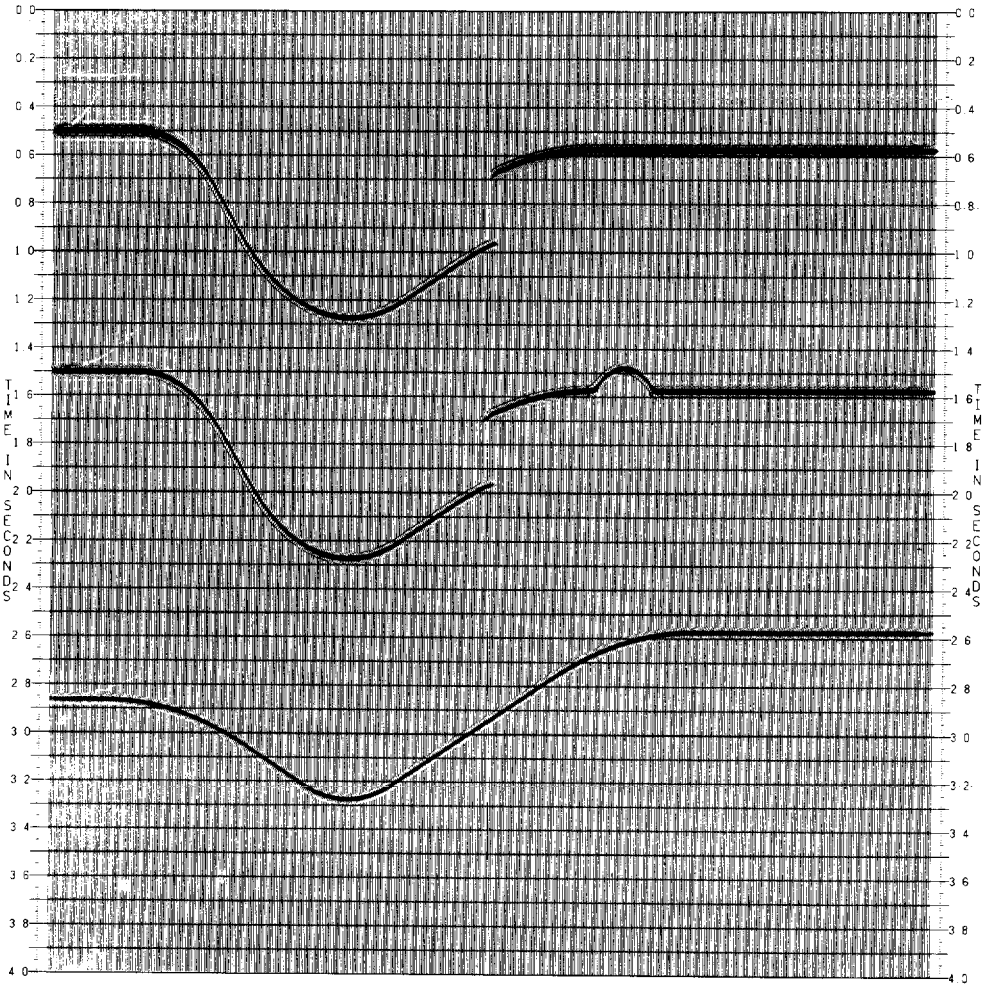

FIG. 18. Model in Figure 16 migrated at 7600 ft/sec, 5 percent low velocity.

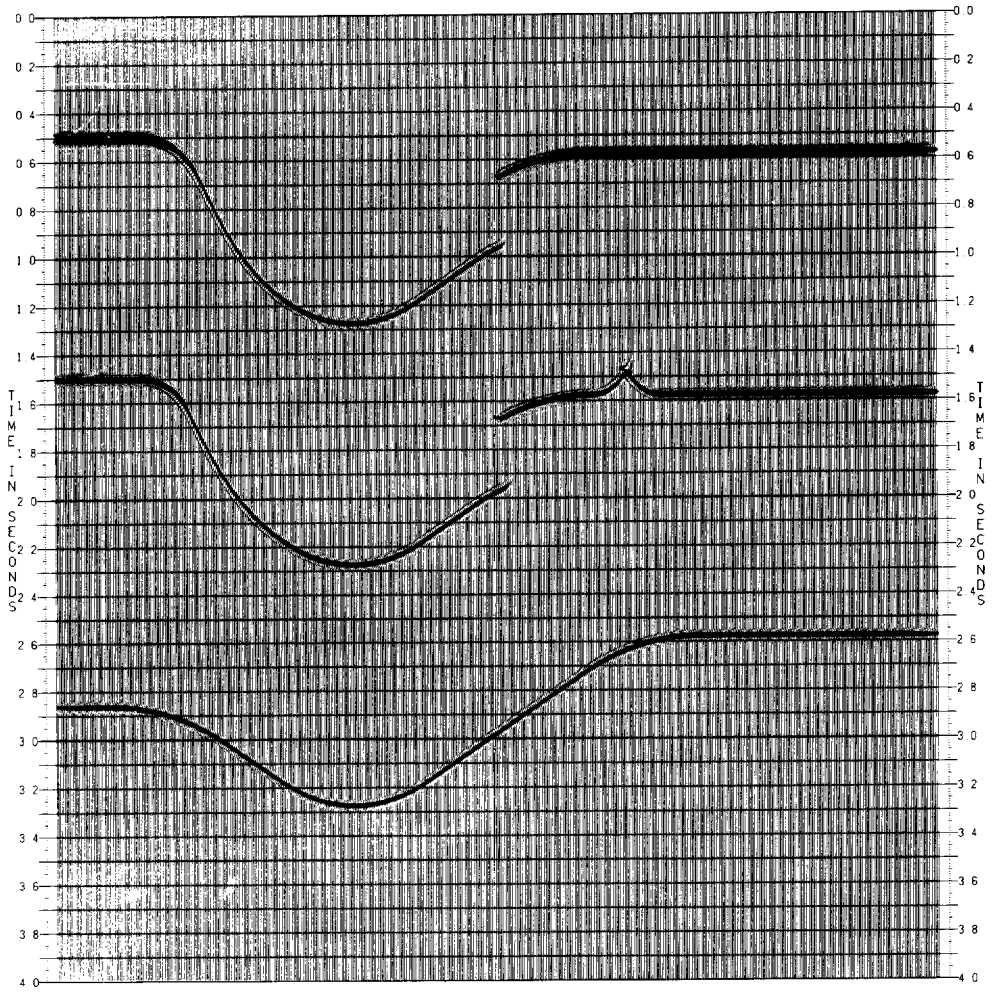

FIG. 19. Model in Figure 16 migrated at 8400 ft/sec, 5 percent high velocity.

can be obtained well beyond 60 degrees. Refinements are possible to improve accuracy at steeper dips by using ray-tracing strategies or modifying the rms velocity as a function of angle to approximate the rms velocity along the ray, which would give the exact result. At present, however, we do not believe these refinements are warranted until further advances are made in estimating velocity with accuracy of the order of 1 percent in structurally complex geologic settings.

Horizontal velocity gradients present an additional complication to both migration and velocity estimation techniques. They can be "handled" from a mechanical point of view in much the same way as are the vertical gradients, by allowing the rms velocity term in the 2-D and 3-D migration algorithms to vary with x, y, and z. The errors in migration caused by lateral velocity gradients are not as well understood as those caused by vertical gradients, and the matter is still being actively researched.

Let us now leave the theory and models and examine several field examples of 2-D and 3-D migration.

FIELD EXAMPLES

The first 2-D migration example comes from the Gulf of Mexico. Figures 28 and 29 show, respectively, the stack section and migrated section. The trace interval is 50 m, typical Gulf velocities were used, and the display bandwidth is about 40 Hz shallow and 20 Hz at depth. Technically the result is very clean with virtually no migration noise or

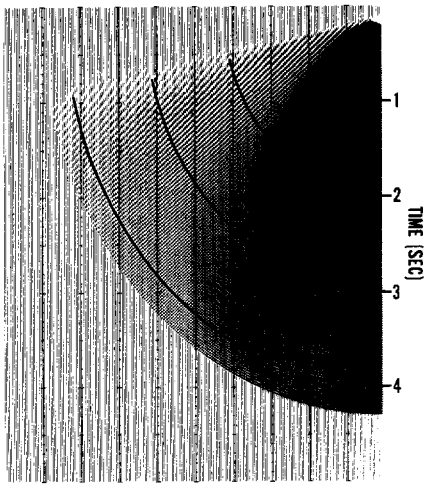

FIG. 20. Migrated 40 Hz sinewave at constant 2500 m/sec velocity.

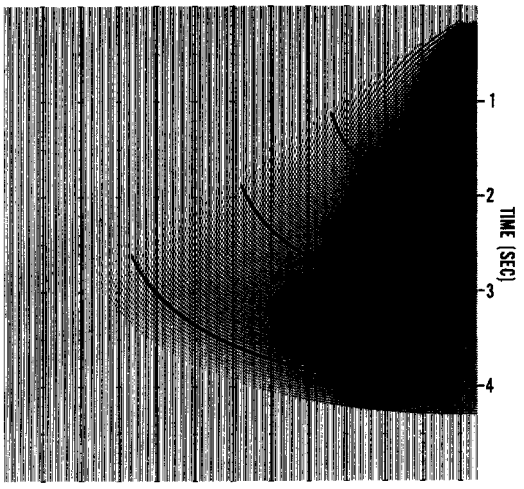

FIG. 21. Migrated 40 Hz sinewave with varying velocity $V = 1800 + 600\ t$ m/sec.

artifacts, and waveform character has been well preserved. Geophysically, the main value of 2-D migration in this example is to enhance fault resolution in the relatively simple sand/shale section. At depth, while some simplification occurs in the structural picture, it would be remarkable if the assumptions for valid 2-D migration were met; that is, sections parallel to this one would look exactly alike.

A second 2-D example comes from the North Sea. The CDP stack and 2-D migrated sections are shown in Figures 29 and 30, respectively. Trace spacing in this case is 25 m and the display bandwidth is higher than in the previous Gulf Coast example. The stacked section exhibits a simple Tertiary-Cretaceous section down to about 1 sec. Below the Cretaceous-Jurassic unconformity the data are complex, discontinuous, and exhibit numerous diffraction events. The 2-D migrated picture reveals a much more interpretable Jurassic section between 1 and 2 sec, indicating major block faulting and tectonic activity probably related to salt movement. In particular, several small fault blocks on the left of the section and also just right of center are virtually obscured by diffractions on the stacked section. After migration, they stand out with remarkable clarity, as does the uncomformity at the base of the Cretaceous. Overall, the waveform and character of the input section are faithfully preserved in the migrated picture, due principally to the wave equation formulation of the algorithm. This is perhaps the most significant difference between this "Kirchhoff" based migration and the earlier diffraction-summation techniques.

Whether the structural picture portrayed here by migration is correct cannot be answered from this result alone; additional seismic control is necessary. In general, from our experience we know complex geology is seldom sufficiently two-dimensional to satisfy the assumptions required for 2-D migration. While French (1975) extends the range of applicability of 2-D migration to both oblique profiles and plunging 2-D structures, there is no substitute for 3-D data and 3-D migration to correctly image seismic returns from complex geologic targets.

Until recently 3-D seismic data acquisition and processing were more of a research curiosity than a practical exploration tool. However, continuing advances in computer hardware and software coupled with innovations in seismic data acquisition over the

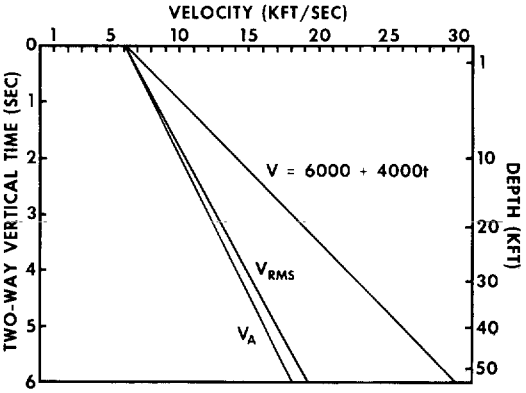

FIG. 22. Velocity function—model 1.

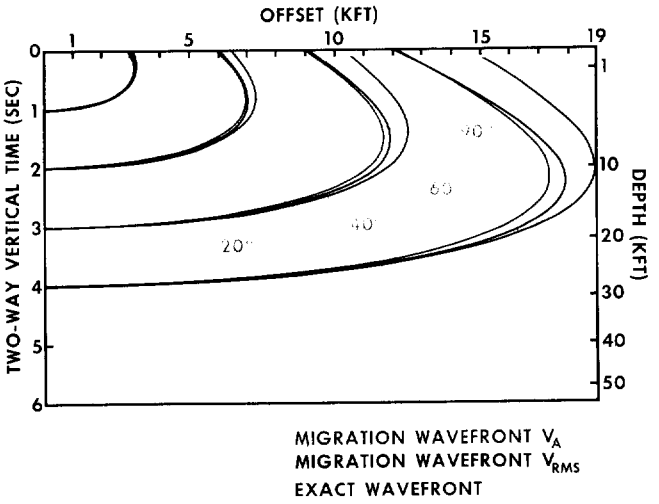

FIG. 23. Wavefront curves for model 1 showing the exact and approximate wavefronts using the average and rms velocities in the Kirchhoff migration integral.

past several years now make it economically feasible to conduct 3-D surveys on both land and marine prospects. Tegland (1976) describes some of these significant advances which include streamer tracking systems to locate accurately the streamer relative to the boat for each shot, and efficient land 3-D collection techniques based on crooked traverses and perimeter shooting. An example of the latter applied to a California land prospect is shown in Figure 32. The technique, called Seisloop/Seisquare[1], obtains 3-D coverage by shooting around regular or irregular loops into geophones emplaced completely around the perimeter of the same loop. In this prospect, 14 rectangular loops covering 10 sq mi were shot using Vibroseis® source patterns at each of the large dots, into geophone arrays at each small dot. Each source-receiver midpoint location is calculated and the corresponding trace assigned to a unique "bin" 330 ft square, resulting in the regular CDP map of Figure 33. Traces common to a bin are stacked together after static and NMO corrections have been applied, yielding a set of stacked traces on a uniform 330 ft x, y grid with an average CDP fold of six. These data may be arranged for display in numerous ways. Figure 34 shows a north-south gather of CDP lines 19, 20, and 21 which are 330 ft apart and about 3 miles long. Data quality is fair to good in the shallow section. The geology is complex showing strong north dip, and well control indicates that the shallow gas production is controlled by numerous small fault blocks. The prospect is an old field with 25 existing wells, generally thought to be drilled out. 3-D seismic was tried in an attempt to uncover additional secondary fault traps in a mature field development situation. As a result of the 3-D survey, five new drilling locations were identified, and as of this writing, two have been drilled and tested commercial gas with recoverable economic value about ten times the cost of the 3-D survey and drilling.

Of major significance in this project was the application of 3-D migration based on the formula of Figure 4 appropriately discretized for sampled data input. Figure 35 shows three output sections from the

[1]Service Mark of GSI. U.S. Patent No. 3,867,713.
®Continental Oil Co.

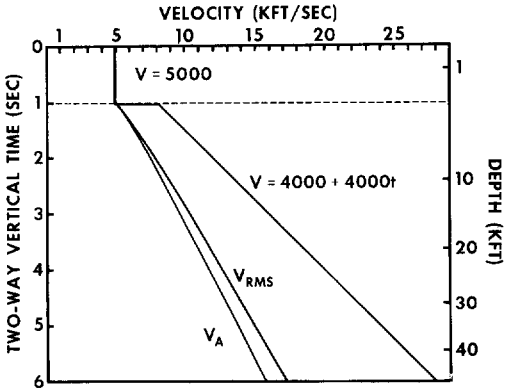

FIG. 24. Velocity function—model 2.

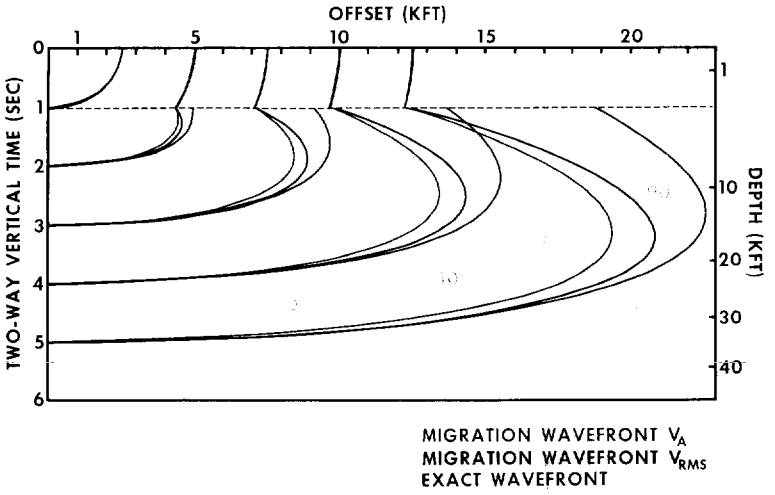

FIG. 25. Wavefront curves for model 2.

3-D migration process at the same locations as the CDP stack lines in Figure 34. Each trace in the migrated picture results from a weighted sum over a square aperture of 10 × 10 input CDP stacked traces. The aperture size was determined by the maximum time dip rates as seen on the stacked sections in the north-south direction and between lines in the east-west direction.

For comparison, Figure 36 shows the same three lines migrated with the 2-D algorithm. The clarity and definition of the 3-D migration are superior to both the 2-D migration and CDP stack at all levels. In fairness to the latter, however, it should be noted that 6-fold conventional shooting is not a very heavy field effort by current standards. Better conventional 2-D results could have been obtained with higher fold shooting. That more conventional seismic would have contributed to finding additional reserves in this field is questionable since several generations of 2-D work had already been exploited to their fullest in discovering the known reserves. The key to finding any remaining pools was dense spatial sampling and accurate location of small untested fault blocks, both of which the 3-D migrated data addressed. Of secondary interest is a major unconformity seen at about 1.5 sec on the 3-D sections, but rather obscure on the CDP and 2-D migrated sections. This unconformity may play a significant role in deeper untested targets in the field. Its expression is more apparent on east-west lines illustrated in Figure 37, showing two 3-D migrated lines gathered across the prospect 660 ft apart. Also evident are numerous north-south trending faults which control the shallow gas production.

Of considerable importance to the overall success of this project was the confidence placed in the 3-D migrated result by the geologist-interpreter because it tied subsurface well control, whereas the stacked sections did not. Finally, in retrospect, the 330 ft bin size was marginally adequate for the exploration objective in terms of structural dip and resolution implications. The space sampling intervals Δx, Δy are critical parameters in 3-D surveys and must be selected to meet the geologic and resolution objectives within the economic constraints imposed on the program. In general, 3-D seismic surveys will,

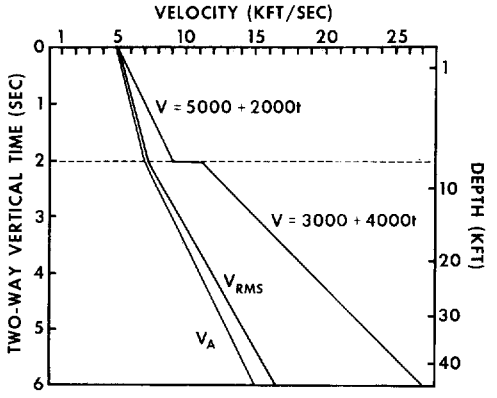

FIG. 26. Velocity function—model 3.

because of their custom problem-solving nature, require a much greater degree of preplanning and client-contractor interplay than conventional seismic surveys.

SUMMARY AND CONCLUSIONS

Our understanding of migration has come a long way from the era of wavefront charts and curves of maximum convexity. We now view the operation as a rigorous inverse wave propagation process subject only to the limitations of the scalar wave equation assumption, and our ability to estimate propagation velocity. Both these areas will undoubtedly be the focal points for further improvements in migration practice in the years ahead.

This discussion has centered on the integral formulation for migration. The finite-difference school also has its advocates and supporters and no attempt was made here to plead their case. Loewenthal (1974), Koehler (1976), Larner (1976), and others have discussed the latter in considerable detail. To claim one approach is vastly superior to the other is to ignore the fact that both integral and finite-difference migrations are based on the scalar wave equation. In the limit of no approximations in implementation they would yield the same results.

In the author's opinion, the integral method offers the following advantages:

1) The 2-D and 3-D algorithms can be implemented without approximating the scalar wave equation.
2) Data can be migrated to 90 degrees and beyond, velocity accuracy and cost being the only real limitations.
3) In 3-D applications, departure from a regular x, y grid can be easily accommodated by the integral method. This occurs frequently in both land and marine applications because of the difficulty in collecting seismic data exactly where you want it.
4) Finally, the integral method lends itself more readily to ad hoc weighting schemes which are meant to combat seismic noise not comprehended by any of the current wave equation formulations for migration.

ACKNOWLEDGMENTS

The author wishes to thank his colleagues, Cam Wason and Bruce Secrest, for their many helpful, theoretical discussions relevant to the concepts presented herein. My thanks also go to Frank Linville, Chyi Lu, and Bob Hester for their assistance in preparing the model results. And, finally, the author is grateful to Texas Instruments for permission to publish this work.

REFERENCES

Berryhill, J. R., 1976, Diffraction response for nonzero separation of source and receiver: Geophysics, v. 42, p. 1158–1176.

Claerbout, Jon F., 1970, Coarse grid calculations of waves in inhomogeneous media with application to delineation of complicated seismic structure: Geophysics, v. 35, p. 407–418. *(Text continued on p. 76)*

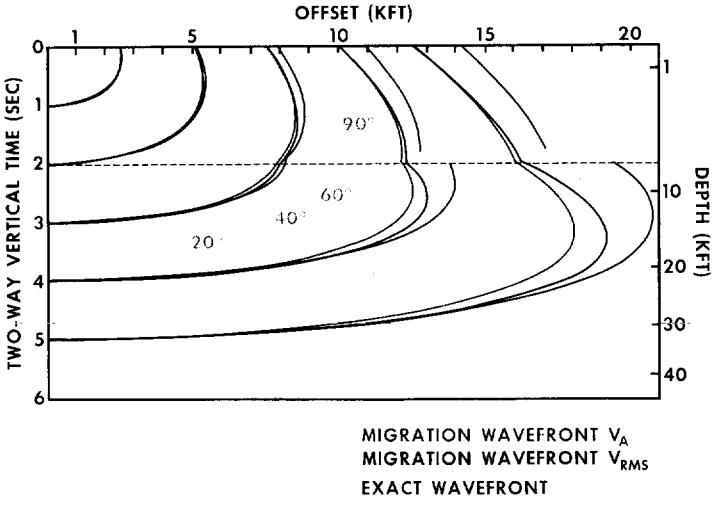

FIG. 27. Wavefront curves for model 3.

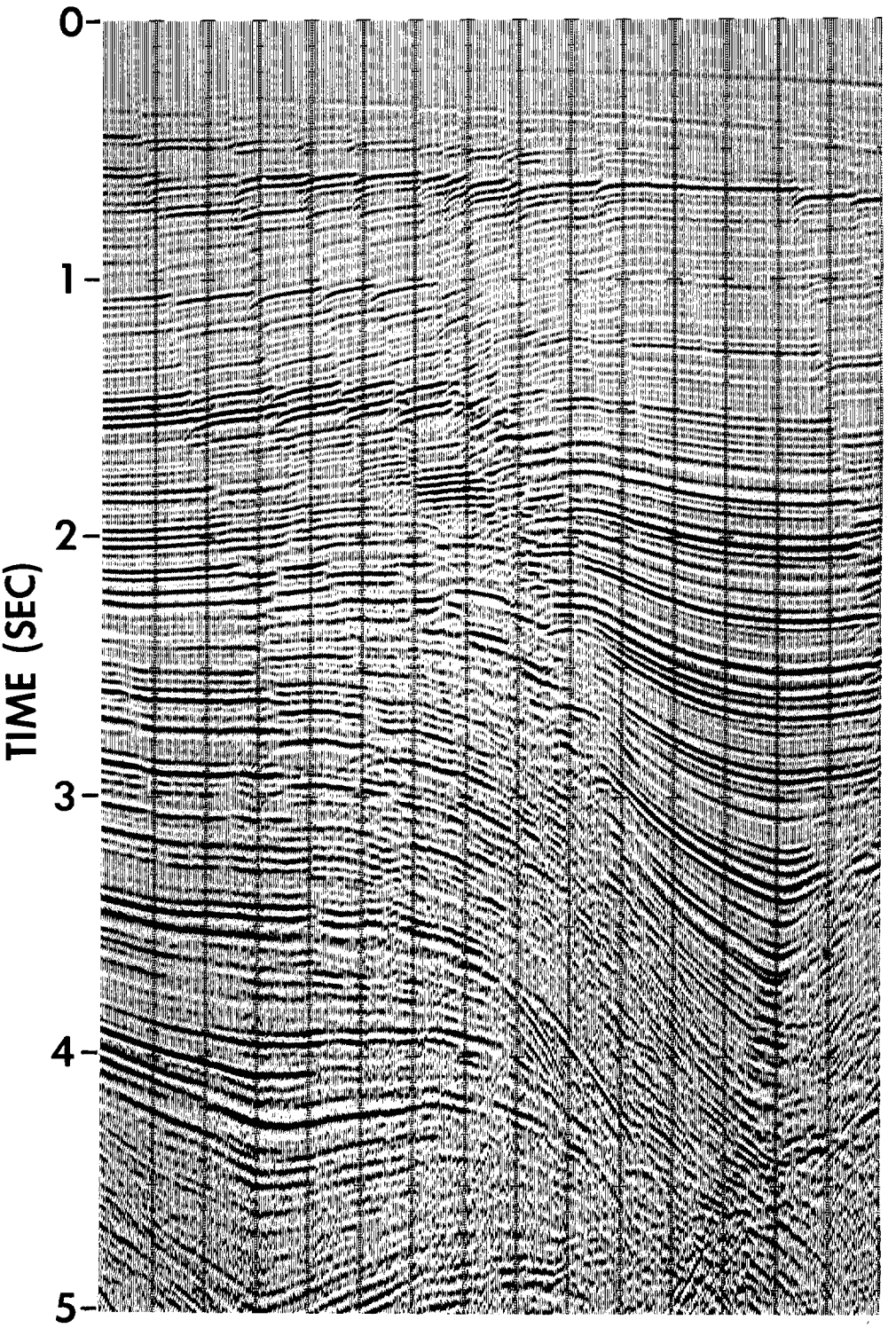

FIG. 28. Gulf of Mexico CDP stacked section.

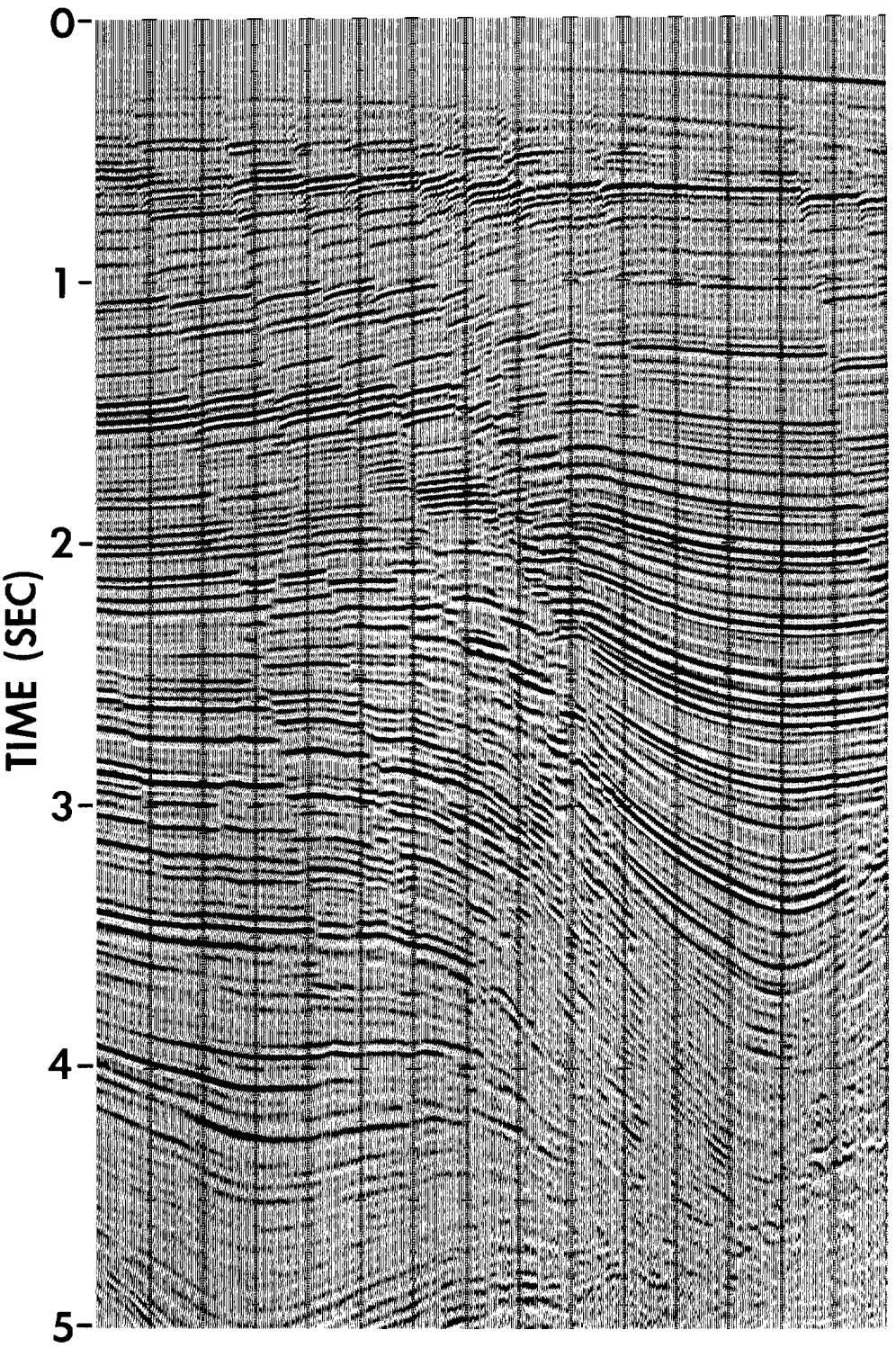

FIG. 29. Gulf of Mexico 2-D migrated section.

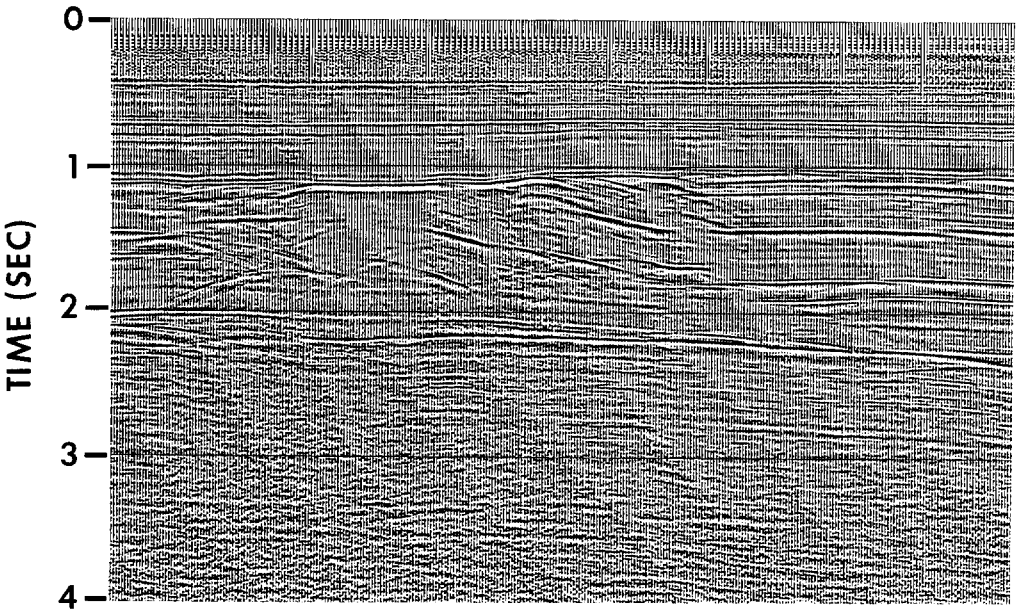

FIG. 30. North Sea—stacked section.

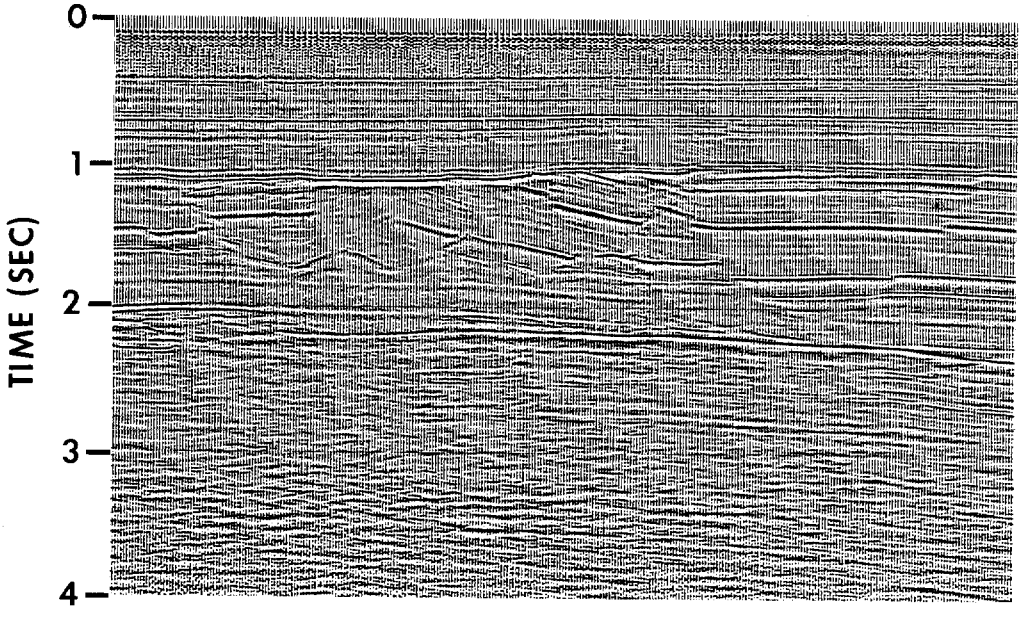

FIG. 31. North Sea 2-D migrated section.

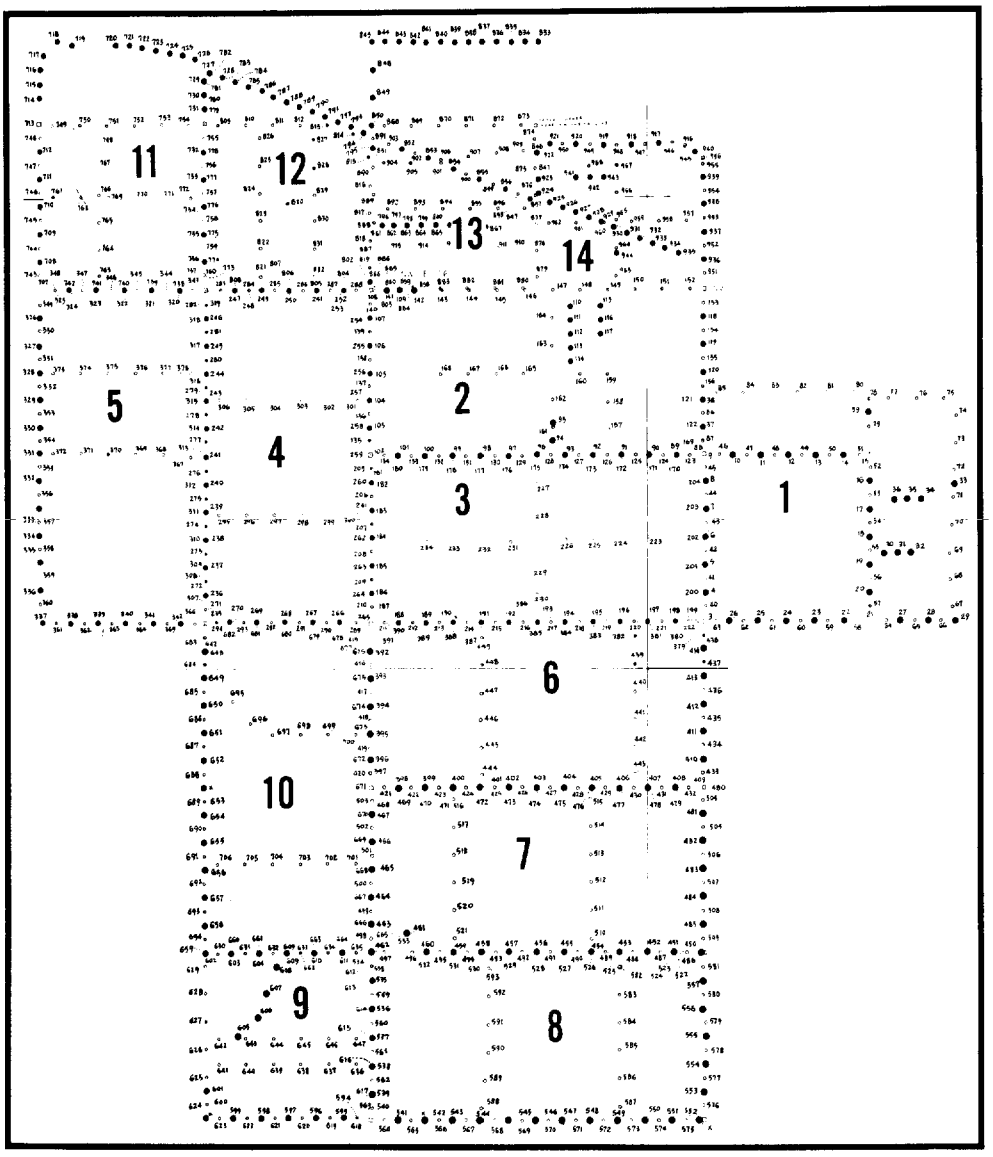

FIG. 32. California land 3-D prospect map showing location of source and receiver positions.

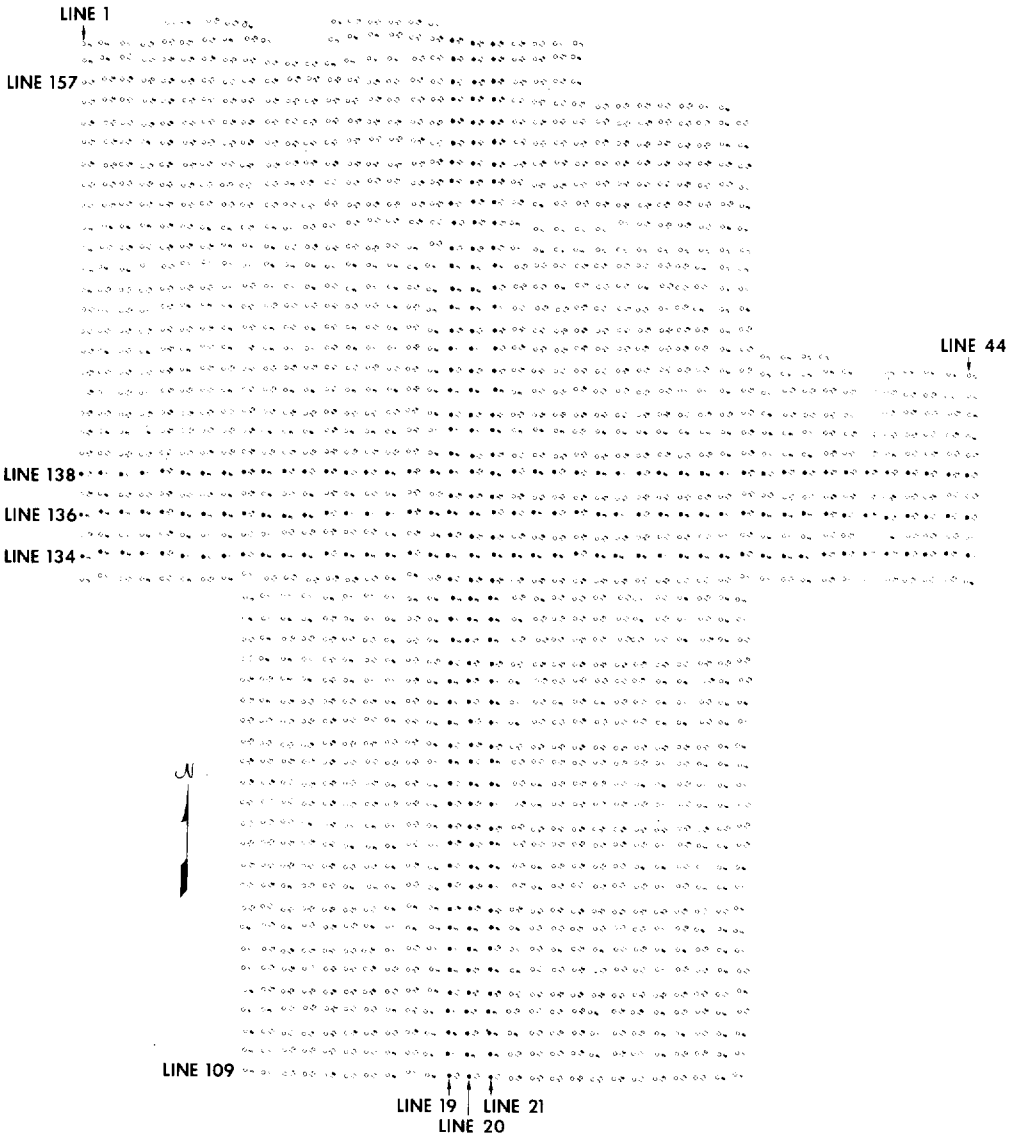

FIG. 33. California land 3-D prospect map showing grid of CDP bin center locations.

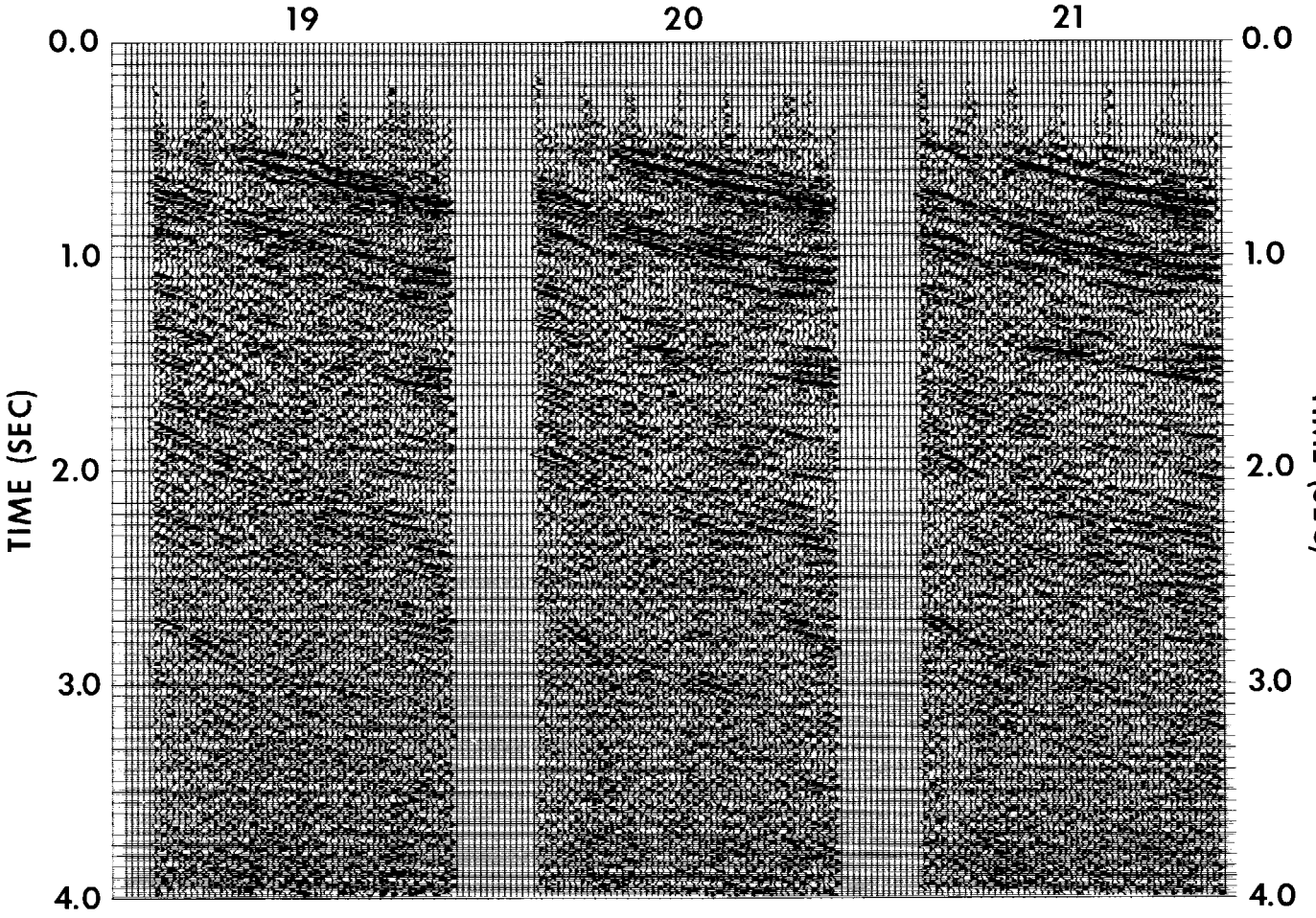

FIG. 34. California land 3-D prospect showing three north-south CDP stack sections 330 ft apart.

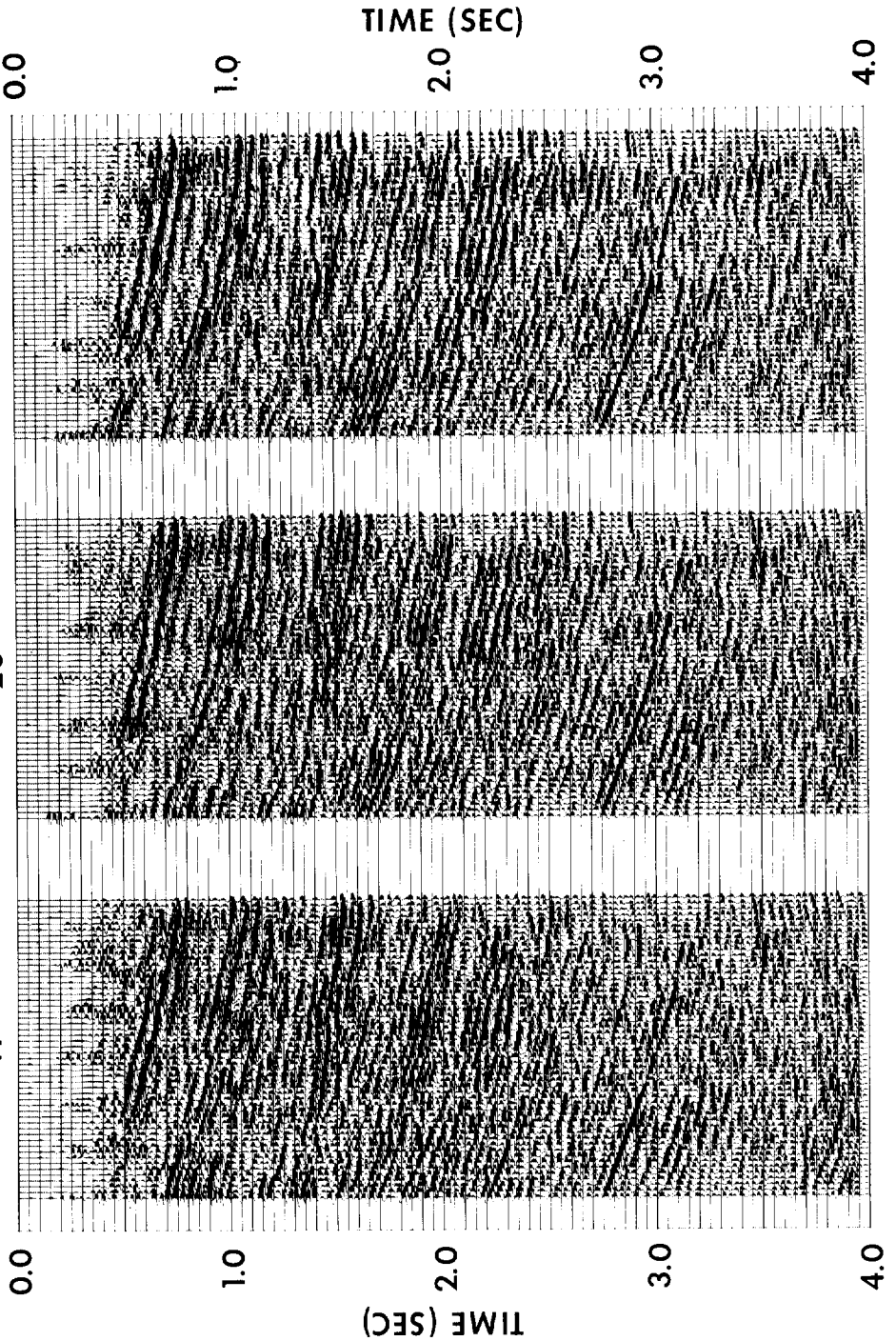

FIG. 35. 3-D migrated sections corresponding to the CDP stack sections in Figure 34.

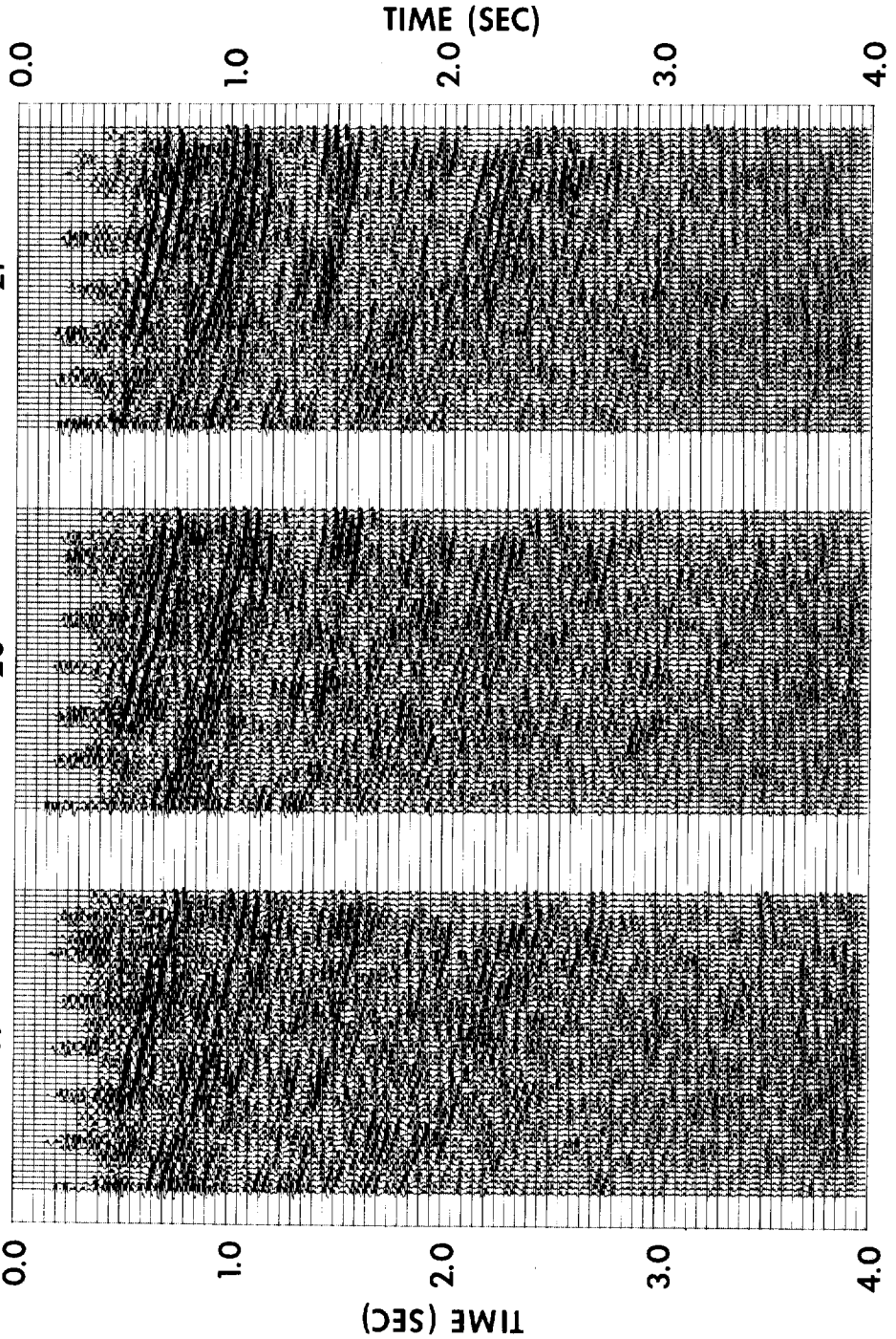

FIG. 36. 2-D migrated sections corresponding to the CDP stack in Figure 34.

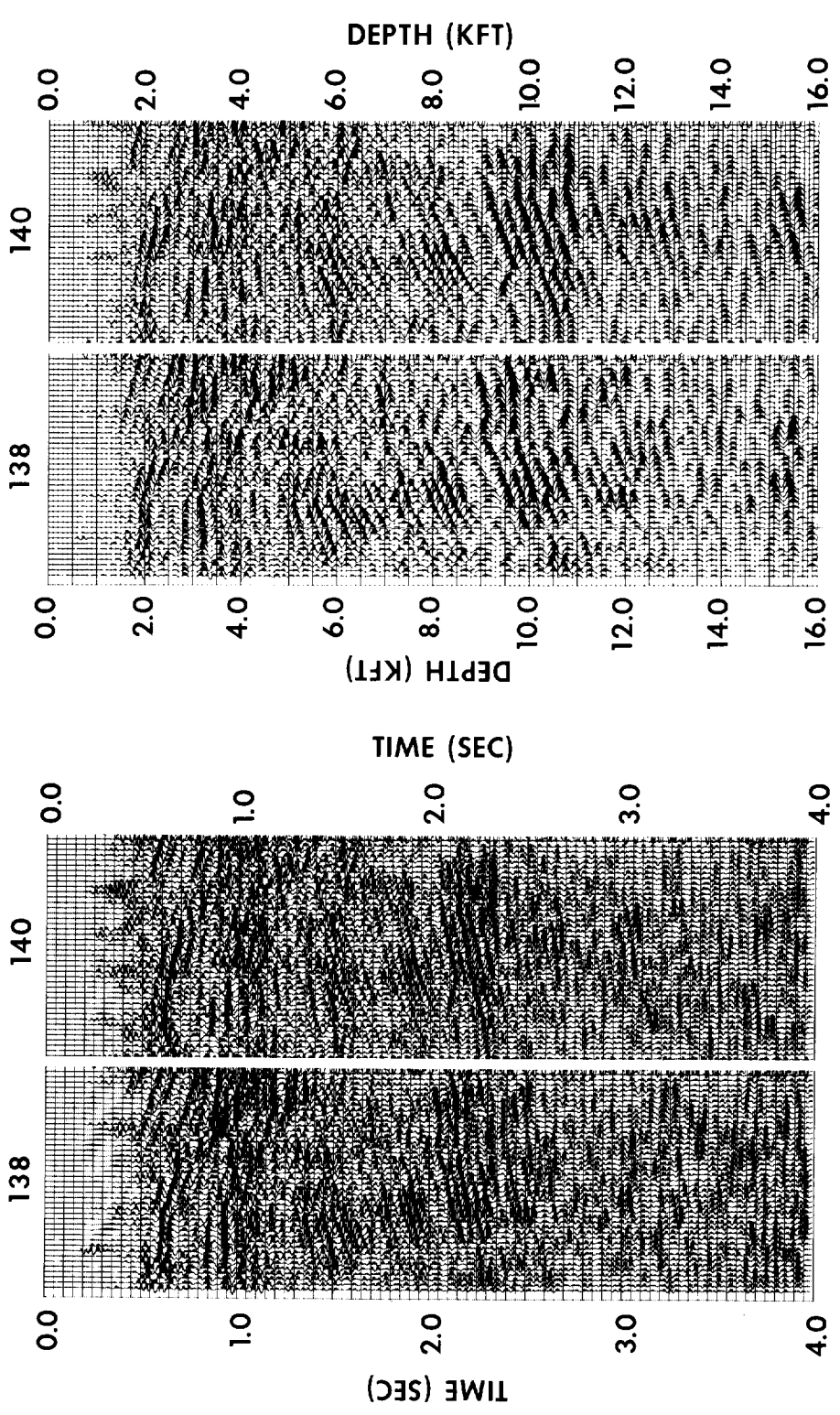

FIG. 37. 3-D migrated sections gathered in an east-west direction across the prospect. 660 ft apart. Left pair in migrated time. Right pair in migrated depth.

——— 1976, Fundamentals of geophysical data processing: New York, McGraw-Hill Book Co., Inc.
Claerbout, Jon F., and Doherty, S. M., 1972, Downward continuation of moveout corrected seismograms: Geophysics, v. 37, p. 741–768.
Dohr, G. P., and Stiller, P. K., 1975, Migration velocity determination: Part II. Applications: Geophysics, v. 40, p. 6–16.
French, W. S., 1975, Computer migration of oblique seismic reflection profiles: Geophysics, v. 40, p. 961–980.
Goodman, J. W., 1968, Introduction to Fourier optics: New York, McGraw-Hill Book Co., Inc.
Hagedoorn, J. G., 1954, A process of seismic reflection interpretation: Geophys. Prosp., v. 2, p. 85–127.
Hilterman, F. J., 1970, Three-dimensional seismic modeling: Geophysics, v. 35, p. 1020–1037.
——— 1975, Amplitudes of seismic waves—a quick look: Geophysics, v. 40, p. 745–762.
Koehler, F., and Reilly, M.D., 1976, Interpretational benefits of wave equation migration: Presented at 46th International SEG meeting, October 27 in Houston.
Kuhn, M. J., and Alhilali, K. A., 1976, Weighting factors in the construction and reconstruction of acoustical wavefields: Geophysics, v. 42, p. 1183–1198.
Larner, K., and Hatton, L., 1976, Wave equation migration: two approaches: Presented at 46th International SEG meeting, October 24 in Houston.
Loewenthal, D., Lee, L., Robinson, R., and Sherwood, J., 1974, The wave equation applied to migration and water bottom multiples: Presented at 44th International SEG meeting, November 12 in Dallas.
Magnus, W., and Oberhettinger, F., 1954, Formulas and theorems for the functions of mathematical physics: New York, Chelsea Publishing Co.
Morse, P. M., and Feshback, H., 1953, Methods of theoretical physics, Parts I and II: New York, McGraw-Hill Book Co., Inc.
Musgrave, A. W., 1961, Wavefront charts and three-dimensional migration: Geophysics, v. 26, p. 738–753.
Sattlegger, J. W., 1975, Migration velocity determination: Part I. Philosophy: Geophysics, v. 40, p. 1–5.
Tegland, E. R., Bone, M. R., and Giles, B. F., 1976, 3-D high resolution data collection, processing and display: Presented at 46th International SEG meeting, October 27 in Houston.
Timoshin, Y. V., 1970, New possibilities for imagery: Soviet Physics—Acoustics, v. 15, p. 360–367.
Trorey, A. W., 1970, A simple theory for seismic diffractions: Geophysics, v. 35, p. 762–784.
Walter, W. C., and Peterson, R. A., 1976, Seismic imaging atlas 1976: United Geophysical Corp. publication.

APPENDIX

The system response function $H(k_x, k_y, \Delta z, \omega)$, which translates the scalar wave field across a slab of thickness $\Delta z = z - z_0$ in a constant velocity medium, is given by the 3-D Fourier transform of the convolutional operator given in equation (7). Therefore, we have

$$H(k_x, k_y, \Delta z, \omega) = -\frac{1}{2\pi}\frac{\partial}{\partial z}\iiint dx dy dt \frac{\delta(t - r/C)}{r} e^{-i(\omega t + k_x x + k_y y)},$$

and integrating over t gives

$$H = -\frac{\partial}{\partial z}\int dy \left[\frac{1}{2\pi}\int dx \frac{e^{-i\frac{\omega}{c}\sqrt{(z-z_0)^2 + x^2 + y^2}}}{\sqrt{(z-z_0)^2 + x^2 + y^2}} e^{-ik_x x}\right] e^{-ik_y y}.$$

The inner integral is a Hankel function of the second kind (Magnus and Oberhettinger, 1954) thus we are left with the following integral over y:

$$H = -\frac{\partial}{\partial z}\int dy - i\pi H_0^{(2)}\left(\sqrt{\left(\frac{\omega}{c}\right)^2 - k_x^2}\sqrt{(z-z_0)^2 + y^2}\right) e^{-ik_y y}.$$

Now using the relation between cylindrical functions

$$H_0^{(2)} = J_0 - iN_0$$

where J_0 and N_0 are Bessel and Neumann functions, respectively, we substitute for $H_0^{(2)}$ in the y integral and evaluate the final transform as (Magnus and Oberhettinger, 1954)

$$H = \frac{\partial}{\partial z}\left[\frac{\sin(z-z_0)\sqrt{\left(\frac{\omega}{c}\right)^2 - k_x^2 - k_y^2}}{\sqrt{\left(\frac{\omega}{c}\right)^2 - k_x^2 - k_y^2}} + i\frac{\cos(z-z_0)\sqrt{\left(\frac{\omega}{c}\right)^2 - k_x^2 - k_y^2}}{\sqrt{\left(\frac{\omega}{c}\right)^2 - k_x^2 - k_y^2}}\right]$$

$$= i\frac{\partial}{\partial z}\frac{e^{-i(z-z_0)\sqrt{\left(\frac{\omega}{c}\right)^2 - k_x^2 - k_y^2}}}{\sqrt{\left(\frac{\omega}{c}\right)^2 - k_x^2 - k_y^2}}$$

$$= e^{-i(z-z_0)\sqrt{\left(\frac{\omega}{c}\right)^2 - k_x^2 - k_y^2}}.$$

The two-dimensional transfer function [equation (11)] can be derived in a similar manner starting with the convolutional operator [equation (10)].